# Chapter 13

## THE DIGISONDE 256 IONOSPHERIC SOUNDER

Bodo W. Reinisch, Klaus Bibl, David F. Kitrosser, Gary S. Sales, Jane S. Tang, Zhao-Ming Zhang, Terence W. Bullett and John A. Ralls

University of Lowell Center for Atmospheric Research, 450 Aiken Street, Lowell, MA 01854, USA

## 1. INTRODUCTION

Some 60 years ago, the first ionosondes were developed based on the experiments by Breit and Tuve [1926]. These were simple instruments that measured the time of flight of pulse-modulated HF signals. In this paper we describe the new scientific applications that the modern digital ionosonde offers. We limit our discussion to the Digisonde 256, since it is the only globally used advanced ionosonde system. The DGS 256 network of some 40 sounders is shown in Figure 1. Nineteen of these sounders are being deployed by the U.S. Air Weather Service and the installation phase should be completed by the end of 1990 [Buchau, 1989]. The Digisonde 256 measures all observables of the ionospheric echoes [Reinisch, 1986]: amplitude, phase, range, frequency, Doppler shift, Doppler spread, angle of arrival, and wave polarization. Real time autoscaling of the ionogram data and calculation of the electron density profiles in ARTIST (Automatic Real Time Ionogram Scaler with True Height) eliminates some of the previously existing difficulties of ionosonde research: the tedious process of ionogram reduction and the time delay and costs associated with the calculation of the electron density profiles. Since the Digisonde can be remotely operated via standard telephone lines it is now relatively easy to prepare a station for special campaigns. A number of analysis techniques that may be useful for the Worldwide Ionosphere/Thermosphere Study have been developed over the last years and are described in Sections 3 to 7. As in the case of incoherent scatter radar research, it requires the involvement of many scientists to develop advanced analysis techniques and the corresponding software to make more extensive use of the observational techniques of the Digisonde 256. Section 2 summarizes the measuring techniques of the Digisonde system; for details we refer to the Digisonde Manual [Bibl et al., 1981].

## 2. THE DIGISONDE 256 SYSTEM

### General Layout

Designed as a pulse radar system with a wideband 10 kW peak power transmitter and precise fast-switching frequency synthesis, the Digisonde 256 covers a frequency range from 0.5 to 30 MHz. A wideband transmit antenna with a vertical beam aperture of about 90° for vertical sounding and a log-periodic antenna for oblique and backscatter sounding are used in alternation. For reception an array of seven spaced crossed-loop antennas allows the polarization and the angle of arrival of ionospheric echoes to be measured. The array is laid out as an equilateral triangle with one antenna at its center; the aperture is nominally 100 m.

The sounder is installed in a rack and an equipment desk (Figure 2). The six foot rack houses the 10 kW transmitter, the uninterruptible power supply, and the antenna switch to which the seven receiving antennas are connected. The desk holds the transceiver/processor, ARTIST, tape drive, printer, and modems.

### System Operation

The system operates in a number of different modes: ionogram, fixed frequency, and drift. In the ionogram mode, the sounder steps through the selected frequency band in increments of 5, 10, 25,

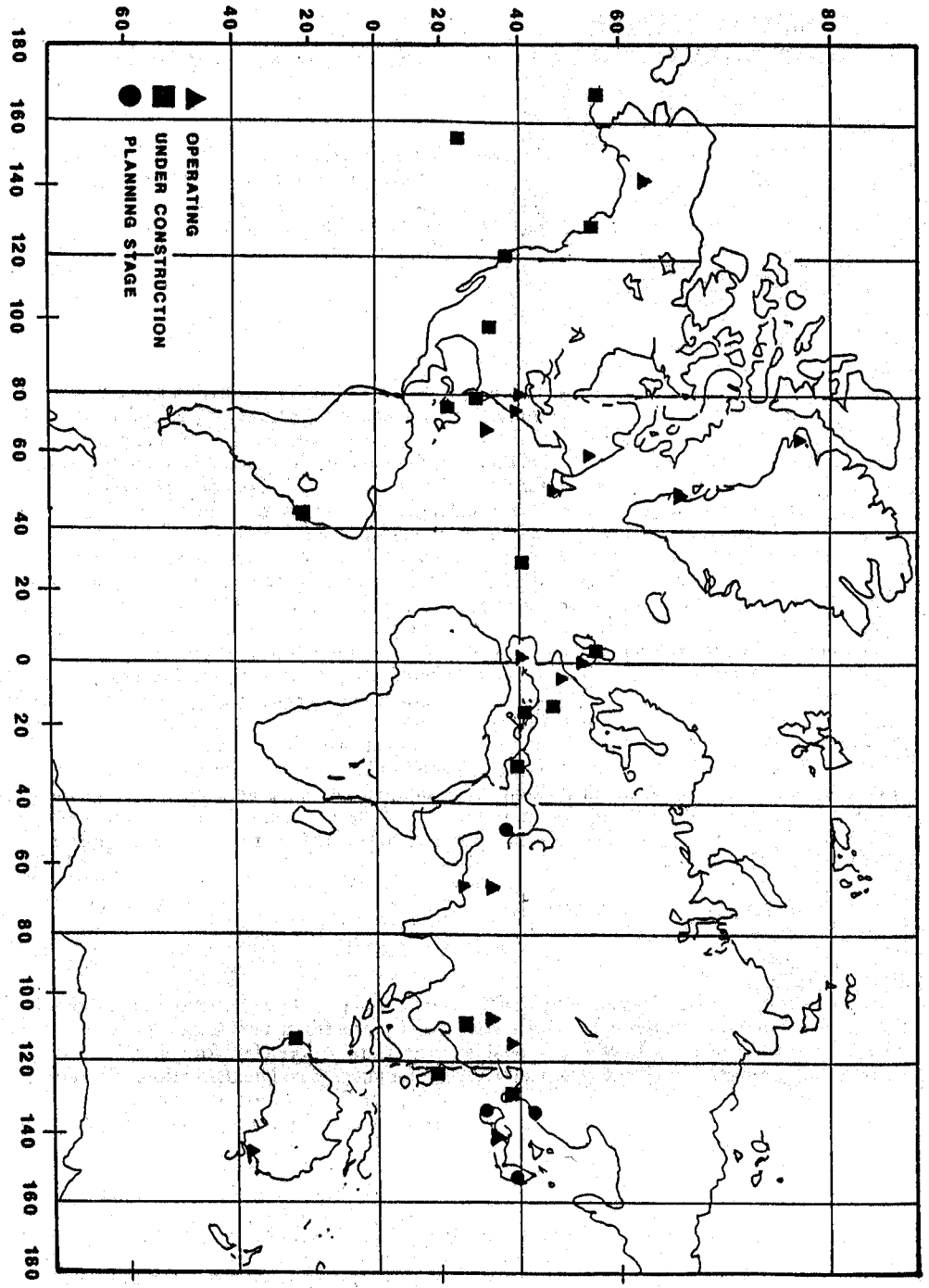


Figure 1 -- Global network of Digisonde 256 digital ionospheric sounders as of September, 1989.

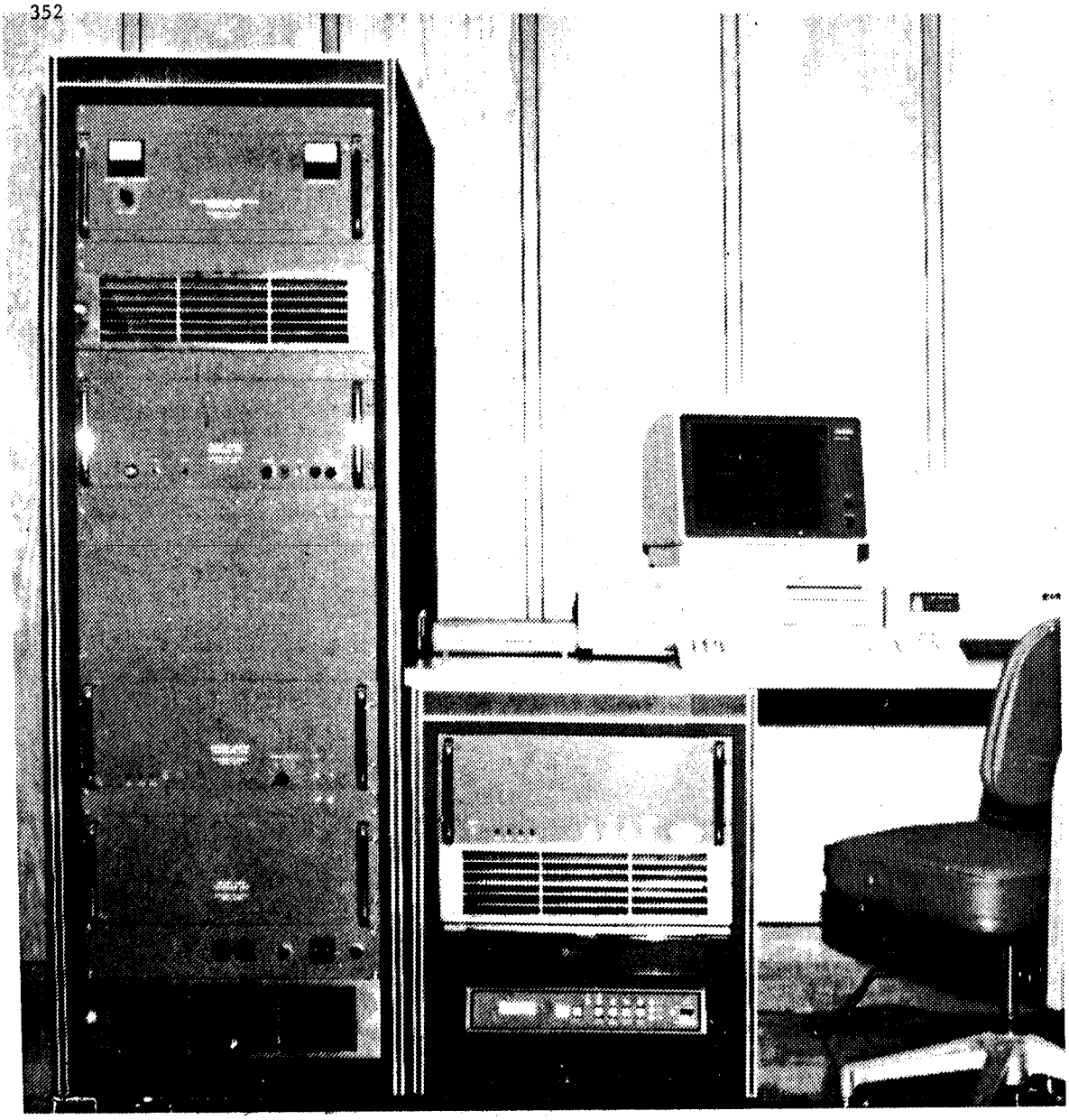

Figure 2 -- The Digisonde 256. The six foot tall rack on the left contains the 10 KW final amplifier and its pulsed power supply, the 7 receive antenna switch and the uninterruptible power supply. The desk rack (center) contains the transceiver/signal processor and the 9 track tape drive. Located on top of the desk is the ARTIST ionogram scaler and its associated printer and modem.

50, 100 or 200 kHz. The lower and upper frequency limits are 0.5 and 30.0 MHz. Although logarithmic frequency scans are available, they are rarely used and most systems operate with 100 kHz increments for vertical incidence ionograms. The time dwell on each frequency determines the Doppler resolution of the discrete Fourier Transform, and must be appropriately selected for different ionospheric conditions. Typical values for the dwell lie between 0.5 and 2.0 seconds, resulting in Doppler resolutions of 2 to 0.5 Hz. The Digisonde ionograms have either 128 or 256 height ranges, and for each range a 16 point Doppler spectrum is calculated (8 points only for 256 height ranges). It is difficult to visually present an ionogram that is composed of 128 spectra for each sounding frequency. The situation becomes more complicated when incidence angle and signal polarization are considered. To get an indication where the echoes in the ionogram are coming from, the antenna beam of the receiving array is steered from vertical (where it receives both in O and X polarization) to several off zenith directions. Up to 12 azimuthal directions can be scanned for each of two zenith angles, 10° or 21°. The different directions and the O/X switching are time sequenced at the pulse repetition rate, and only one receiver is used.

The decision was made, somewhat arbitrarily, to limit the number of observations or "channels" to 16, e.g. 16 Doppler lines for the ordinary polarized signals, or eight Doppler lines each for O and X polarization, or just two Dopplers each for six incidence angles and the vertical O and X channels. To preserve the full information content all 16 channels must be recorded on magnetic tape, and one data block with 4096 bytes per sounding frequency is written onto the 1600 bpi tape. Generally this is not done, however, since a 2400' tape can only store about 50 of these full information ionograms. Instead, the 16 channels for each frequency/range bin are analyzed, the channel with the maximum amplitude is selected, and the amplitude and channel number, or "status", is recorded. This technique makes it also possible to present the ionogram in the conventional frequency versus range frame, as illustrated in Figure 3.

The sequence of soundings is freely selectable and the system can be preprogrammed to change to a different sequence at any desired day and time. For example, many stations change from the routine 15 min ionogram/drift sequence to a 5 min sequence for the Regular World Days. Different ionogram programs can be preprogrammed and the system will sequence through them as well as through fixed frequency or drift observations. The printout uses an optically weighted font [Bibl and Reinisch, 1978] to present the amplitudes of the overhead ordinary echo traces; the letter X represents the extraordinary traces, and little arrows point to the direction from where oblique echoes are received. On the Millstone Hill (42°N geogr.) ionogram in Figure 3, F region echoes from the south were received at around 8 MHz, and Es echoes from north-east at 3 MHz. The lettering within the ionogram was added for this publication.

The fixed frequency mode is identical to the ionogram mode, except the sounding repeats on the same frequency a selectable number of times. It is also possible to step through four different frequencies, and repeat these transmissions n times. Recording format and the printouts are the same as in the ionogram mode. The drift mode, on the other hand, is very different in its operation and is explained in some detail in Section 5.

## Signal Processing

The received RF signals are amplified in tuned circuits, enabling successful signal reception in regions with high HF communication activities, and converted to an intermediate frequency (IF) of 225 kHz. A 12 bit digitizer takes quadrature samples of the linear IF signal. In the ionogram mode 128 or 256 pairs of quadrature samples are taken which are spaced by 16.66, 33.33, or 66.66 μsec corresponding to 2.5, 5.0, or 10.0 km height resolution, and resulting in range coverages varying from 320 to 1280 km. By using the phase difference between simultaneously transmitted signals, offset in frequency by 5, 15 or 30 kHz, a group path accuracy of better than 1 km can be obtained. For high pulse repetition rates (200, 100, and 50 Hz are available) higher order echoes can fall into the digitizing windows. However, the bi-phase pulse sequence modulation, impressed onto the transmitted signal, results in significant suppression of these high-order echoes during the phase coherent spectral integration process. The symmetric bi-phase sequence code has been optimized for all different ionogram and fixed-frequency programs so as to

```
+------------------------------------------------------------------+
+      ULCAR - MILLSTONE HILL, WESTFORD, MASSACHUSETTS             +
+            LAT 42.6, LONG 71.5W      DIP 72.9  fH 1.4           +
+      DIGISONDE 256 - V5.02.89     UNIVERSITY OF LOWELL, USA      +
+------------------------------------------------------------------+

STATION YEAR DAY H  M     OUT OPT R  E  Q CAR XLZT NRW HEIG PROGRAM
  042   1989 137 12:59 UT 1084100 01-12 1 33E 41D3 334 1239    1

FOF2  FOF1  H'F   H'F2  M3000 FMIN  FOES  MUF   FMINF
 7.8   ***   208.  ****  2.65   1.8   3.5  20.7   3.6

FXI   FMINE FOE   H'E   H'ES  QF    QE    FF    FE
 8.7  1.6   3.5   95.   95.   ***    5.    .2    .4
AUTOSCALED TRACES (KM):
-----------------------
 3. ***** ***** ***** ***** ***** *****  238.  220.  223.  213.
 4.  218.  218.  228.  238.  243.  253.  253.  258.  263.  268.
 5.  273.  278.  288.  293.  308.  318.  328.  333.  338.  343.
 6.  348.  353.  358.  363.  368.  373.  378.  388.  398.  408.
 7.  418.  433.  448.  468.  488.  518.  548.  593.  653.
 1. ***** ***** ***** ***** ***** *****   85.   85.   85.   90.
 2.   90.   90.   90.   95.   95.   95.  100.  100.  100.  105.
 3.  105.  110.  115.  120.  130.  150.

NORMALIZED AMPLITUDE AS AT REFLECTION HEIGHT 100KM IN (DB)
      TOPF    2    3    4    5    6    7 (MHz)
 F      29    0    0   52   63   67   65
 E      20   44   30
 ES     20   44   30

PROFILE - ULCAR
---------------
   W =   5.1  KM
   FSTART PEAK HT   A0       A1       A2       A3       A4     DEV    ROOTS
    (MHZ) (KM)     (KM)     (KM)     (KM)     (KM)     (KM)  (KM)/PT
E     .199  95.655 -25.059   6.677    2.988                     2.8
F1
F2  3.510 297.625-170.479 -34.788  14.060  -6.518    .857  10.8   -
```

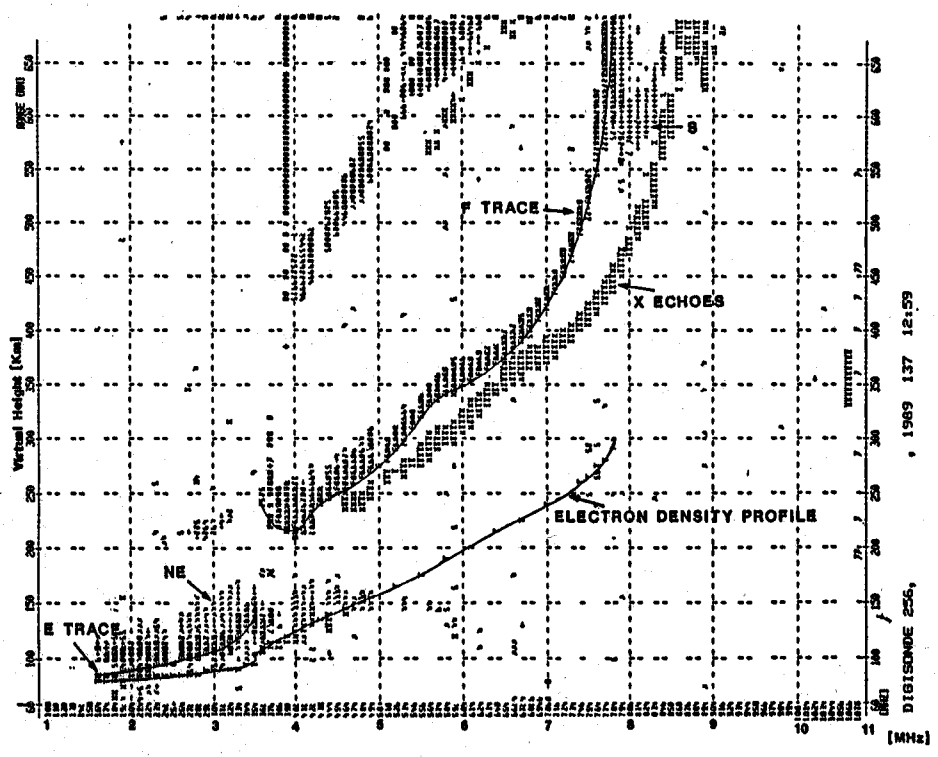


Figure 3 -- The Digisonde 256 on-line ionogram printout includes (from top to bottom) information on the station of observation, system settings, scaled ionospheric parameters, autoscaled trace points, reflection amplitude information and electron density profile parameters. The ionogram is displayed in the lower half of the figure and indicates the ordinary and extraordinary traces, oblique signals with their directions (S, NE) and the calculated electron density profile. Lettering and lines were added for publication. This data is from Millstone Hill, MA at 07:59 LT on 17 May 1989.

suppress these multiples as well as coherent internal noise and external interferers. To avoid the strongest interferers, the Digisonde employs a frequency search technique. Prior to transmission of a frequency $f_O$, the Digisonde listens at frequencies $f_O$, $f_O$ + 10 kHz, and $f_O$ + 20 kHz and uses the one with the lowest interference level as sounding frequency.

A 20-bit discrete Fourier transform calculates the complex spectrum (amplitude and phase) for all height ranges in real time. In the ionogram mode 16 spectral lines are calculated, less when polarization and angle of arrival are measured. In the drift mode up to 256 spectral lines for a limited number of range gates are determined. The spectral data are outputted onto tape and paper; the available amplitude and phase resolution is 0.25 dB and 1.4° respectively.

To handle the large range in signal amplitudes which vary with frequency and range and are controlled by focussing effects, diurnal variation in absorption and geomagnetic activities, the dynamic range of the receiver system has been enlarged to 100 dB by using time-dependent (day/night) and signal-dependent digital gain control. Coherent integration of echoes from three pulses transmitted prior to the actual sample pulses sets the optimum gain level for the integration period thus keeping the gain constant during the coherent spectral integration.

Oblique Ionogram Sounding

Oblique sounding studies between Digisondes separated by distances of 350 to 5000 km have been conducted [Reinisch et al., 1984]. These soundings can be made either in the ionogram or the fixed-frequency mode. Figures 4 and 5 show examples from recent experiments between Goose Bay and Millstone Hill, a distance of 1400 km. In Figure 4 the sequence of afternoon ionograms on 24 August 1989 starting at 1420 LT (1920 UT) indicates a build-up of the F2 propagation mode and the decline of the F1 ledge. The late evening sequence in Figure 5 shows the decay of the F layer. An automatic scaling algorithm for oblique ionograms over distances of 3000 km or less is currently being developed and will result in a quasi-parabolic description of the mid-point vertical electron density profile [Kuklinski et al., 1988].

The internal timing of the Digisonde is controlled by timing pulses that are derived from the system oscillator, which for bistatic sounding is a rubidium standard with a stability of 1 part in $10^{11}$. The clocks in the two Digisondes must be synchronized with an external one second pulse to make oblique ionograms. We are currently testing an automatic time synchronization technique that locks the Digisonde clock within 10 μs to an external time reference such as the GOES or GPS satellite.

Automatic Scaling of Ionograms

The scaling of ionograms has always been a time consuming process that required well trained personnel. A fairly detailed understanding of ionospheric radiowave propagation is required to properly interpret the ionograms. Even the experts have often difficulty in analyzing ionograms in the presence of spread F and oblique signals. This task has become much easier with Digisonde ionograms that identify each echo pixel as either vertical or off vertical, as either O or X polarization. Indeed, now that these signal characteristics are measured it has become possible to automate the routine scaling of ionograms, using an expert system. In the Digisonde 256 the ARTIST software [Reinisch and Huang, 1983; Tang et al., 1988], running on an IBM AT or clone, determines the leading edges of the ordinary echo traces of the E, Es, F1 and F2 layers, scales the standard ionogram characteristics, shown at the top of Figure 3, and calculates the vertical electron density profile [Huang and Reinisch, 1982] as described in Section 4 of this paper. Depending on foF2, the scaling and true height calculation is generally completed within 20 to 40 sec after the ionogram scan has ended. Currently, ARTIST uses the Microsoft MS DOS 3.2 operating system and is written in FORTRAN 4.01. The US Air Weather Service network, called DISS (Digital Ionospheric Sounding System) still maintains the older software of 1987 (MS.DOS 3.2, Microsoft FORTRAN 3.31). For every routine ionogram, ARTIST scales the following characteristics: foF2, foF1, h'F, h'F2, M3000, fmin, foEs, MUF(3000), fminF, fxI, fminE, foE,

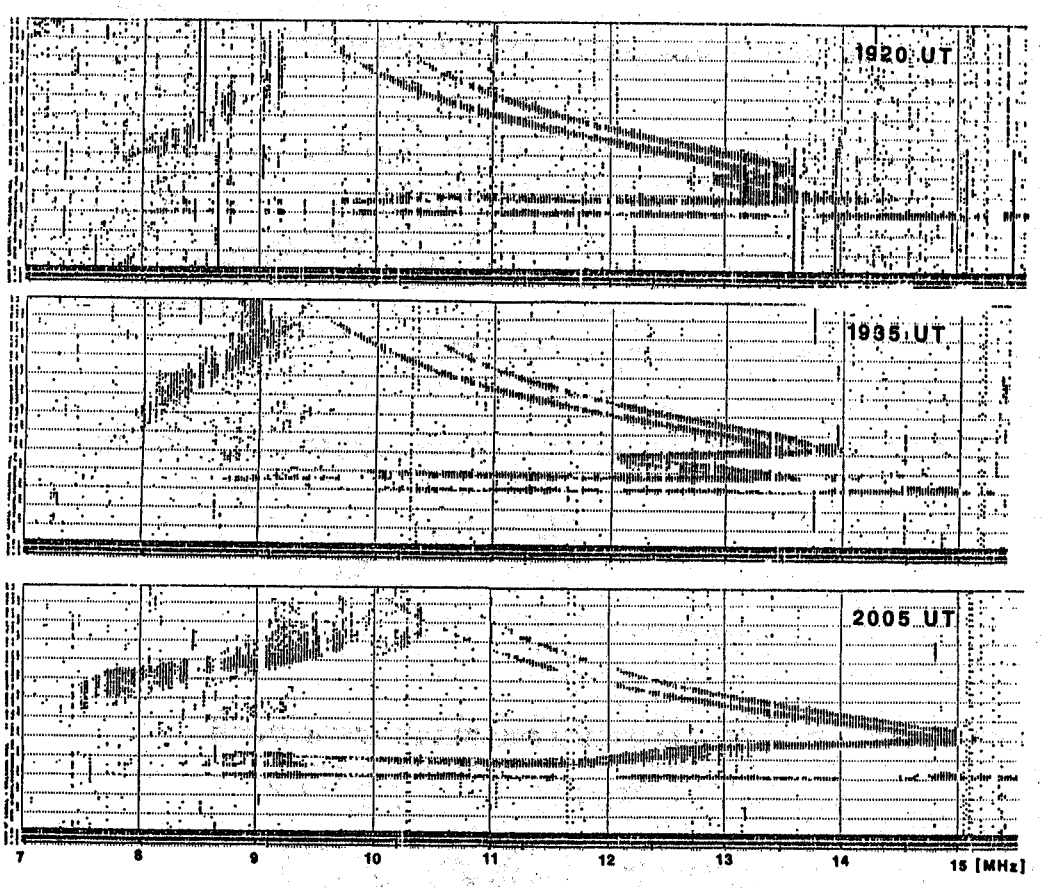


Figure 4 -- Oblique bistatic ionograms from Goose Bay, Labrador to Millstone Hill, MA. This sequence of 3 ionograms was made during the afternoon (19:20-20:05 UT) on 24 August 1989. Single hop E, F1 and F2 as well as two hop F2 reflections are present. The time sequence shows the decline of the F1 layer and an increase of the F2 layer.

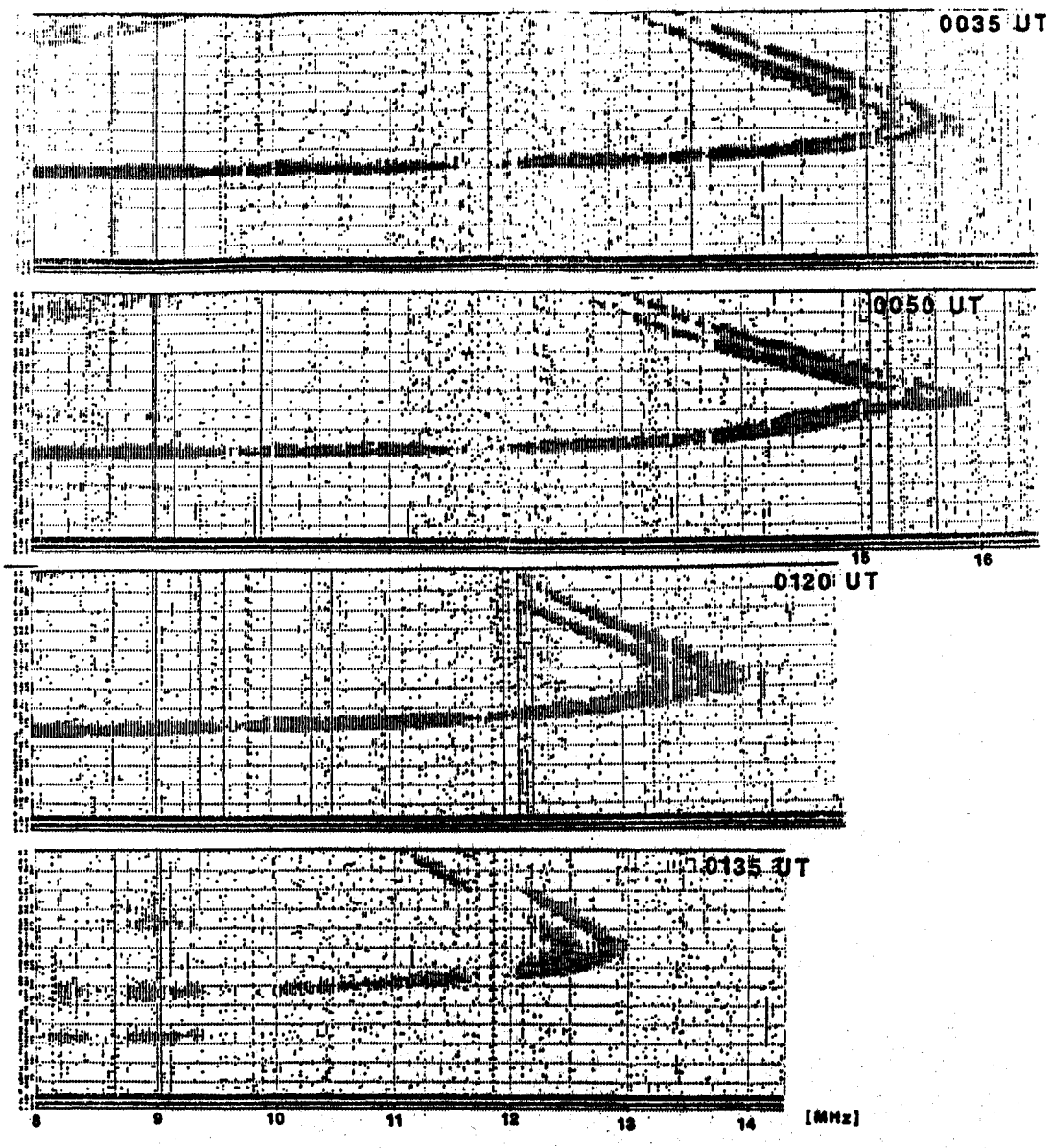


Figure 5 -- Oblique bistatic ionograms from Goose Bay, Labrador to Millstone Hill, MA. This sequence of 4 ionograms was made during the early evening (00:35-01:35 UT) on 24 August 1989. This figure depicts the change in the nighttime F2 region propagation as the evening progresses.

h'E, h'Es, and the average range and frequency spread for E and F traces. The virtual heights of the E and F region echo traces are recorded in km for every 100 kHz frequency increment, together with the echo amplitude and Doppler shift.

The automatic scaling of ionograms makes it feasible to operate at higher data rates, like four ionograms per hour or 12 per hour. The advantage of higher data rates is twofold. For once, fast changes in the ionosphere can be monitored, and secondly there is some data redundancy so that occasional scaling errors have much less weight than in the case of hourly sounding. For the same reason the so-called descriptive and qualifying letters [Piggott and Rawer, 1972] are losing in importance. The high rate data sequence, supplemented by amplitude, Doppler and spread information, generally gives a better description of the ionosphere than could be obtained by hourly readings with descriptive/qualifying letters. The definition of these letters was not made for automatic scaling, and ARTIST does not use any letters. URSI Commission G Working Group G4 during a July 1989 workshop at Lowell, MA, USA, has recommended the data format for automatically scaled ionogram data shown in Table 1.

While autoscaling is a very efficient way of making the most basic ionogram information available for geophysical research it is prone to scaling errors. This issue is addressed in Section 4. Work to further improve the autoscaling is in progress. Recent modifications of the ARTIST algorithms [Tang et al., 1988] have improved the scaling of difficult ionograms. The old ARTIST often failed in the presence of strong multiple Es traces as in the case of the mid-latitude ionogram in Figure 6, where a wrong F trace was identified to start at 1.9 MHz. The new program identifies the F trace correctly with fminF = 4.4 MHz. In the polar cap, the autoscaling had occasionally latched on to improperly identified oblique echoes (Figure 7), the new program avoids this mistake.

Remote Sounder Control and Data Output

One convenient operational feature for scientific applications is the capability to remotely change the operating parameters and the sounding schedule over dial-up phone lines, and to use the same lines for transfer of ionogram data. The Digisonde's ARTIST computer provides two full-featured serial RS232 ports for remote communication at 300, 1200, 1200/75, and 2400 baud via low cost modems and voice grade telephone lines. Most Digisondes are connected to a 2400 baud dial-up modem. Frequently the other full-featured port is connected over dedicated lines to a local terminal at the same facility in another building. In the case of Argentia, Newfoundland, the dedicated line connects the unmanned station to a terminal at the Goose Bay Ionospheric Observatory, some 900 km away. A third serial port is designed to accommodate the special polling procedure of the U.S. Air Weather Service, and to put the ARTIST scaled parameters, trace coordinates, and true height coefficients into a fixed format message. Other users have connected this port or one of the two full-featured ports to another computer for either an automated control function or a remote data gathering application; no additional hardware is required.

The ULCAR Remote Terminal is an IBM PC clone using the same display adapter, monitor, communication hardware, printer and the same software used by the ARTIST for display, printing and communications. The Remote Terminal is connected to one of the two full featured ports over dial-up modems or dedicated lines. Operation of the Digisonde from a Remote Terminal is virtually identical to the onsite operation control. The data output capability is presently limited to the processed ionogram data in the format shown in Figure 3. To make the "raw" 16-channel ionogram and the drift mode data available at the Remote Terminal, requires development of additional software for the ARTIST and the Remote Terminal. Currently available polling features allow the remote user to obtain the last complete ionogram in the format shown in Figure 3, and also the last 24 hourly values of foF2, foF1, and MUF3000. The data base available for polling could easily be expanded.

At the present time eleven Digisondes have dial-up modems attached. Access is generally restricted to those with a direct involvement in the station operation but in principle, access could be made available to the broader scientific community. Addition of operational security software is expected

| Code | Format | Description |
|---|---|---|
| | 80I3 | DATA FILE INDEX |
| 1 | 10F7.3 | GEOPHYSICAL CONSTANTS |
| 2 | 120Z1 | IONOGRAM SOUNDING SETTINGS (PREFACE) |
| 3 | 50F8.3 | SCALED IONOSPHERIC PARAMETERS |
| 4 | 20I2 | ARTIST ANALYSIS FLAGS |
| 5 | 16F7.3 | DOPPLER TRANSLATION TABLE |
| | | O-TRACE POINTS - F2 LAYER |
| 6 | 400I3 | VIRTUAL HEIGHTS |
| 7 | 400I3 | TRUE HEIGHTS |
| 8 | 400I2 | AMPLITUDES |
| 9 | 400I1 | DOPPLER NUMBER |
| 10 | 400F6.3 | FREQUENCY TABLE |
| | | O-TRACE POINTS - F1 LAYER |
| 11 | 150I3 | VIRTUAL HEIGHTS |
| 12 | 400I3 | TRUE HEIGHTS |
| 13 | 150I2 | AMPLITUDES |
| 14 | 150I1 | DOPPLER NUMBER |
| 15 | 150F6.3 | FREQUENCY TABLE |
| | | O-TRACE POINTS - E LAYER |
| 16 | 150I3 | VIRTUAL HEIGHTS |
| 17 | 400I3 | TRUE HEIGHTS |
| 18 | 150I2 | AMPLITUDES |
| 19 | 150I1 | DOPPLER NUMBER |
| 20 | 150F6.3 | FREQUENCY TABLE |
| | | X-TRACE POINTS - F2 LAYER |
| 21 | 400I3 | VIRTUAL HEIGHTS |
| 22 | 400I2 | AMPLITUDES |
| 23 | 400I1 | DOPPLER NUMBER |
| 24 | 400F6.3 | FREQUENCY TABLE |
| | | X-TRACE POINTS - F1 LAYER |
| 25 | 150I3 | VIRTUAL HEIGHTS |
| 26 | 150I2 | AMPLITUDES |
| 27 | 150I1 | DOPPLER NUMBER |
| 28 | 150F6.3 | FREQUENCY TABLE |
| | | X-TRACE POINTS - E LAYER |
| 29 | 150I3 | VIRTUAL HEIGHTS |
| 30 | 150I2 | AMPLITUDES |
| 31 | 150I1 | DOPPLER NUMBER |
| 32 | 150F6.3 | FREQUENCY TABLE |
| 33 | 20I2 | MEDIAN AMPLITUDE OF F ECHO |
| 34 | 20I2 | MEDIAN AMPLITUDE OF E ECHO |
| 35 | 20I2 | MEDIAN AMPLITUDE OF ES ECHO |
| 36 | 20E9.4E1 | TRUE HEIGHT F2 LAYER COEFFICIENTS |
| 37 | 20E9.4E1 | TRUE HEIGHT F1 LAYER COEFFICIENTS |
| 38 | 20E9.4E1 | TRUE HEIGHT E LAYER COEFFICIENTS |
| 39 | 20E9.4E1 | TRUE HEIGHT MONOTONIC SOLUTION |
| 40 | 20E9.4E1 | VALLEY DESCRIPTION |

FORMAT FOR AUTOMATICALLY SCALED IONOGRAM DATA

RECOMMENDED BY URSI WORKING GROUP G4 ON IONOSPHERIC INFORMATICS

TABLE 1

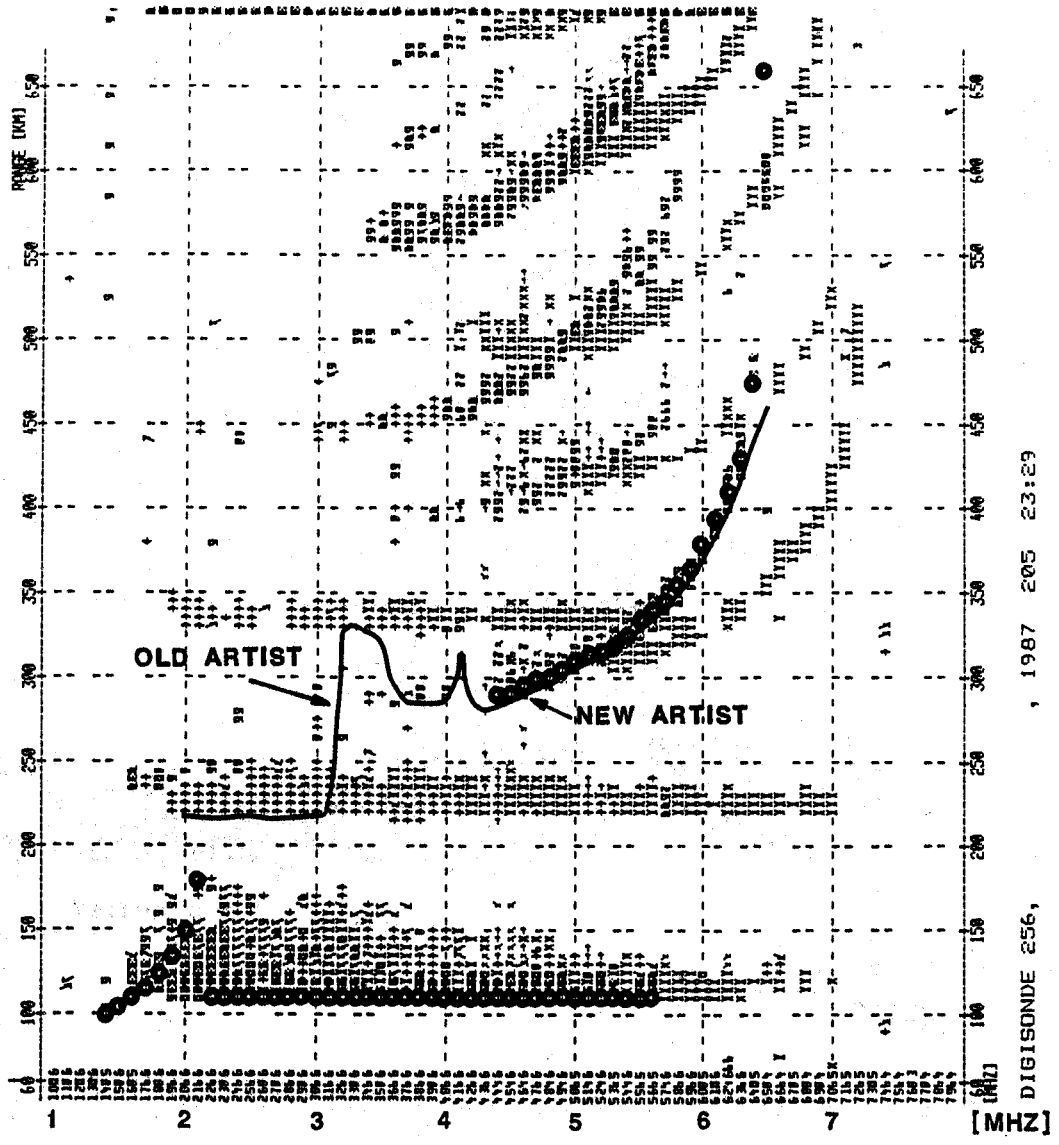


Figure 6 -- ARTIST results indicating the improvement in automatic scaling at mid-latitude stations in the presence of multiple sporadic E reflections. This data is from Millstone Hill at 19:29 LT on 24 July 1987

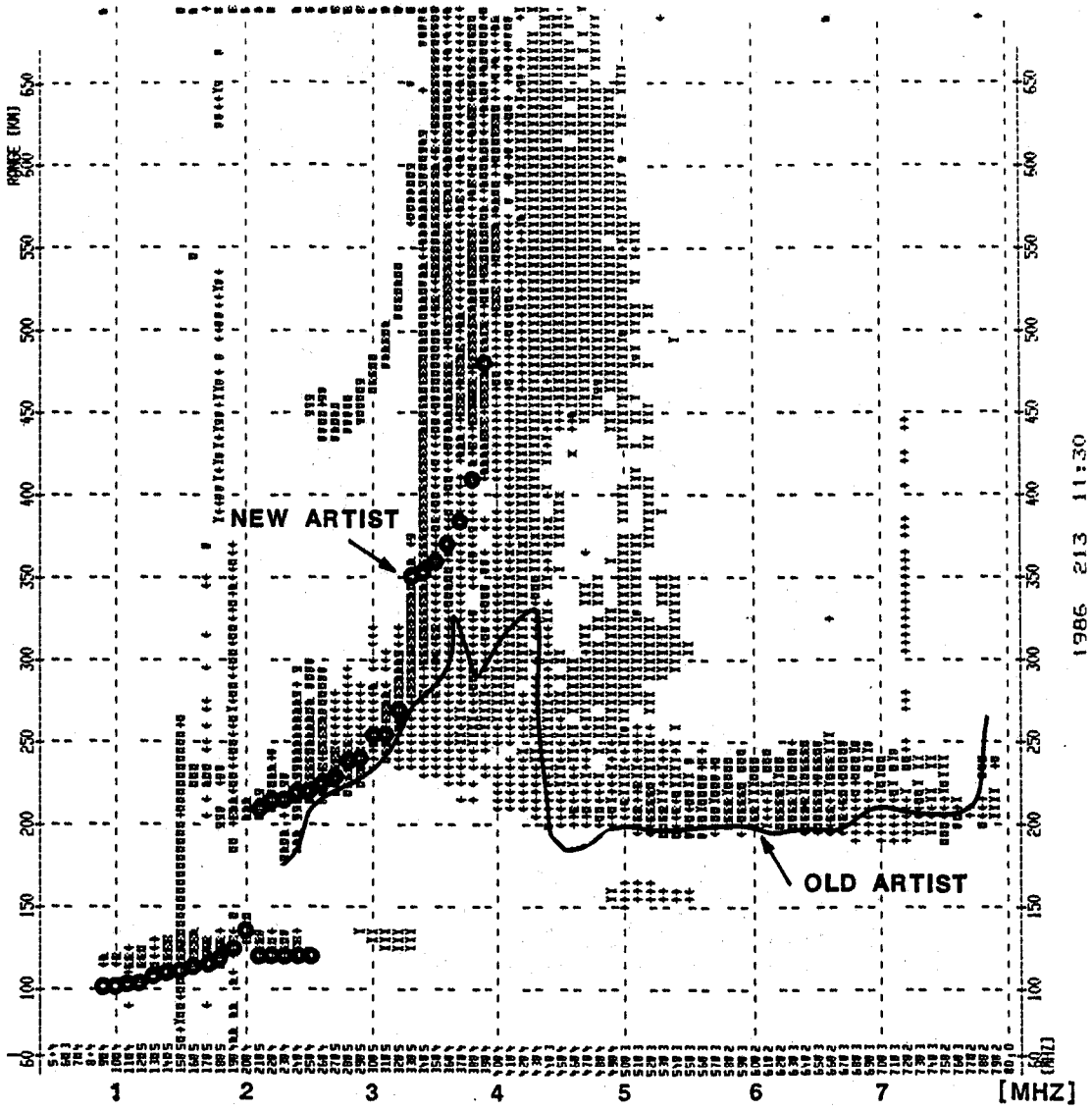


Figure 7 -- ARTIST results indicating the improvement in automatic scaling at high latitude stations during spread-F conditions. This data is from Qaanaaq, Greenland at 14:30 LT on 01 August 1986.

for the near future to protect routine operation of the Digisondes from inadvertent interruption; this will enable broader access to the Digisonde network.

## 3. DESKTOP PROCESSING AND DISPLAY OF IONOGRAM DATA

Ionograms from analog ionosondes were normally recorded on black and white film and no further processing need be done (nor could it be done) to view these data. Furthermore, the information content of these analog ionograms is low, consisting of a 1-bit echo/no echo indication for each frequency/range bin. The Digisonde ionograms, on the other hand, are available on magnetic tape in computer-readable form, containing the multiparameter information described in Section 2. Software for a desktop computer (an amended IBM AT, configured like the on-line ARTIST equipment, with added color display and color ink jet printer) has been developed which makes it possible to display, edit, and print the multiparameter ionograms, scaled characteristics, and the electron density profiles as function of time.

This ionospheric data management and analysis software system, called ADEP (for ARTIST Data Editing and Printing),reads the ionogram data and ARTIST-scaled ionospheric characteristics from magnetic tape, and displays the digital ionogram along with the scaled traces and characteristics on a color monitor for the purpose of data analysis or rescaling. Any scaling errors in the autoscaled traces or characteristics can be corrected before the data are written to an archive data file (Table 1) for further study or global data exchange. This "editing" of the ARTIST data can be performed on an ionogram-by-ionogram basis or in a search mode where the magnetic tape is stopped only when specified inconsistencies in the data sequence are detected.

To show the diurnal variations in the ionosphere ADEP plots all quarter-hour ionograms for an entire day on one sheet as illustrated in Figure 8 for Millstone Hill on 20 February 1988. In this example the extraordinary and oblique echoes are suppressed giving a clearer view of the overhead plasma frequency and height variations. These ionogram surveys are helpful in identifying absorption events and the passage of irregularities. The onsets of the high latitude F-region trough and the auroral oval can easily be detected. F-region patches [Buchau et al., 1983], driven across the polar cap by the ExB drift, show as sudden increases in foF2 in the sequence of ionograms.

For ionosphere/thermosphere studies the coupling between different height regions is better seen on the time evolution of the electron density distributions than on the sequence of ionograms. ADEP uses the ARTIST profiles to generate contour plots for 24 hour periods like the example in Figure 9. These contour plots contain the most important information obtained from a day's worth of ionograms. The isodensity contours are represented by contour lines with 0.5 MHz increments in plasma frequency. The data are plotted versus universal time (UT), and local midnight (M), noon (N) and sunrise/sunset in the F and E region (F and E) are marked at the bottom and on top. The peak height of the F layer, hmF, is plotted as a dotted curve. The row of double dots in the lower part of the figure, labeled DATA AVAILIBLITY, indicates the times when ionograms were recorded (upper dot) and whether an electron density profile was calculated (lower dot). In the upper part of the figure the critical frequencies foF2, foF1, foE and foEs are plotted. The vertical lines on the curves specify the extend of the measured frequency spread.

For modeling and predictions, monthly data displays are more suitable than the daily presentations, since they reveal the day-to-day variations much quicker.. An example for a monthly display is given in Figure 10. Here the deviations of foF2 from the quiet-day median is plotted for Argentia, Newfoundland, December 1986. For reference, the Kp indices, obtained from World Data Center A, are plotted above the foF2 data.

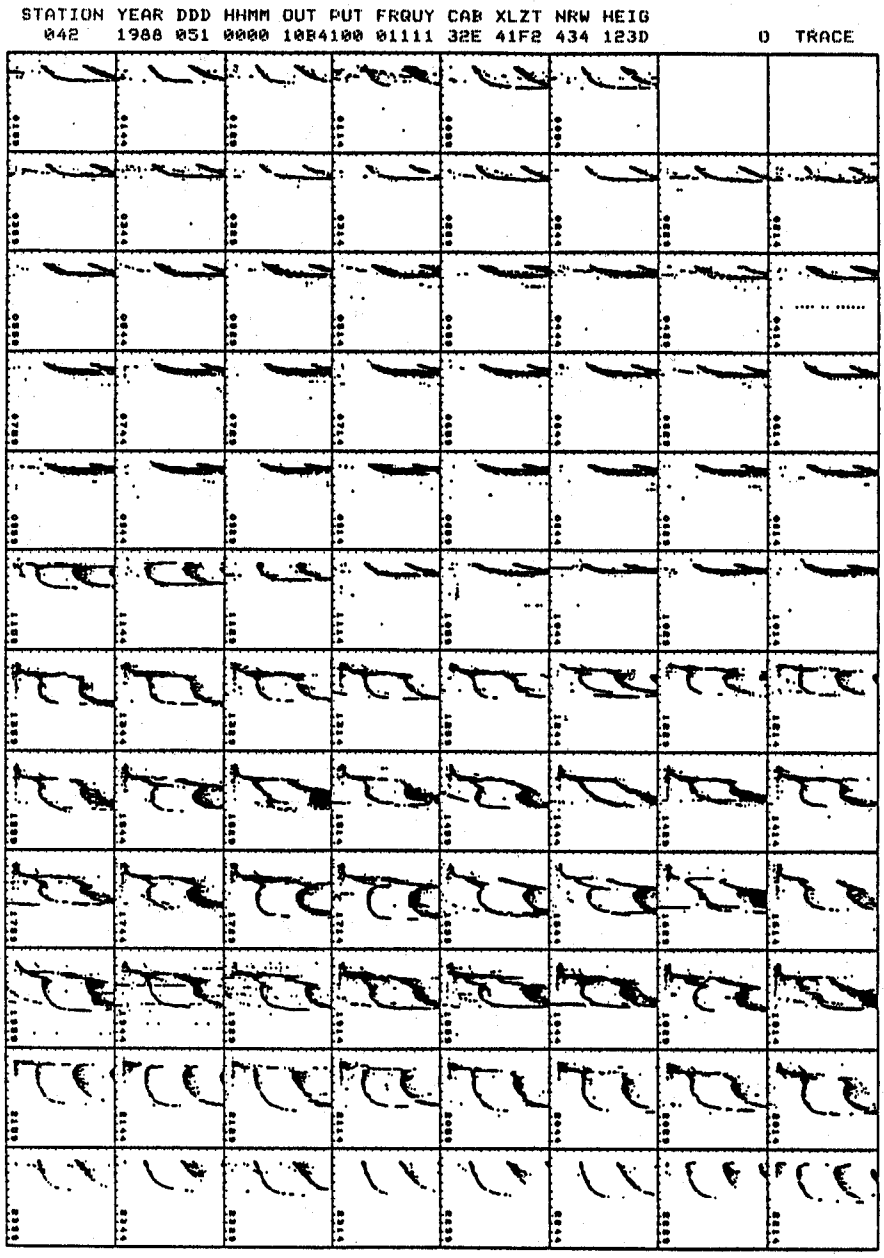


Figure 8 -- Ionogram survey for 20 February 1988 from Millstone Hill, MA. The ordinary component is displayed while the extraordinary and oblique signals are suppressed. Ionograms are shown at 15 minute intervals over a 24 hour period from 00:00 UT to 23:59 UT (19:00 LT to 18:59 LT).

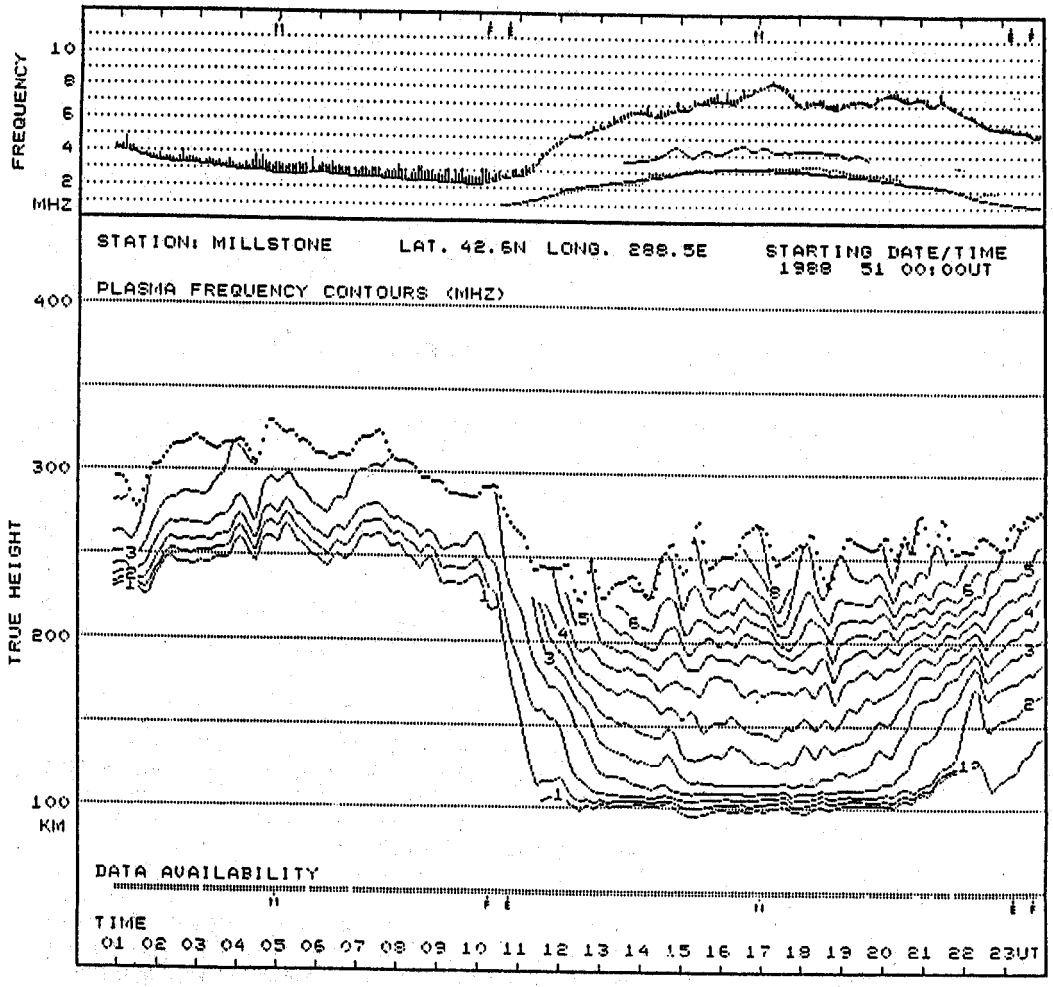


Figure 9 -- Plasma frequency contours vs time for 20 February 1988 from Millstone Hill, MA. The top panel indicates foF2, foF1, foE and foEs over the 24 hour period from 00:00 UT to 23:59 UT. The bottom panel shows plasma frequency contours in true height and time. Contour lines are spaces at 0.5 MHz intervals. The data availability line indicates the presence of data as well as local noon, midnight, and sunrise/sunset in the E and F regions.

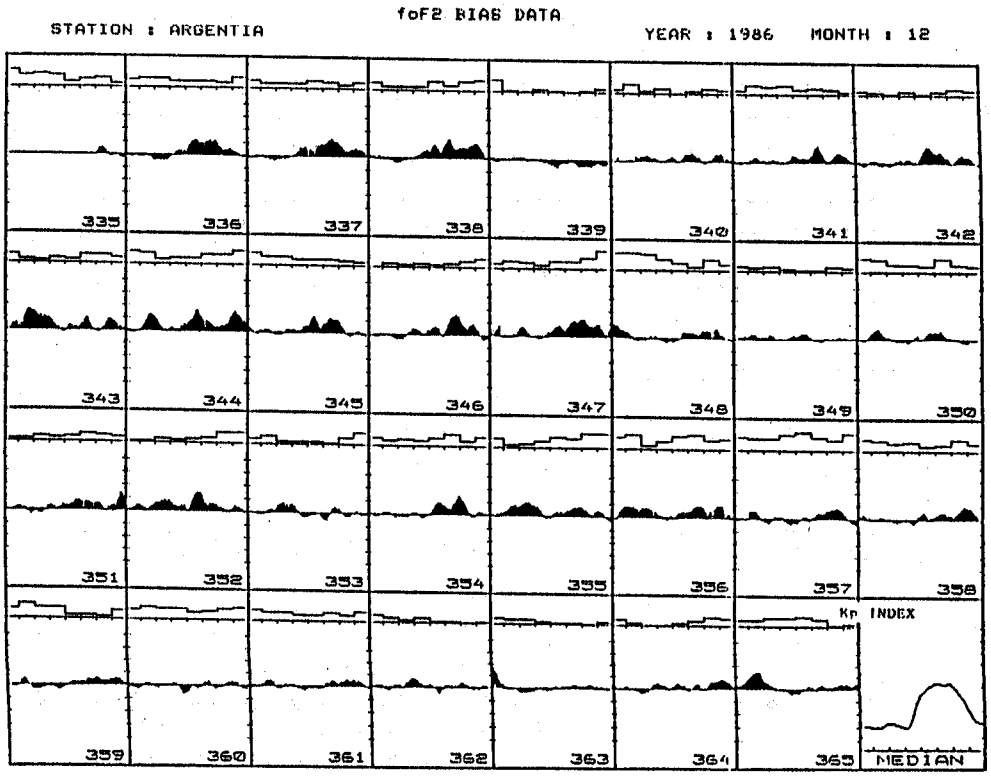


Figure 10 -- Daily display of foF2 deviations from the monthly median for December, 1986. This data is from Argentia, Nfld. Plotted above each daily foF2 deviation is the Kp index for that day. The last panel in the lower right shows the monthly median values (for quiet days) from which the deviation is calculated.

## 4. REAL TIME ELECTRON DENSITY PROFILES

ARTIST directly converts the autoscaled traces into a vertical electron density profile; the time required is approximately 20 sec. In the inversion process, the electron density profile in each ionospheric region (E, F1 and F2) is given as [Reinisch et al., 1988; Huang and Reinisch, 1982]

$$Z(f) - Z(f_s) = A_{I+1} + g^{1/2} \sum_{i=0}^{I} A_i T_i^*(g) \qquad (1)$$

$$g = \frac{\ln f/fc}{\ln fs/fc} \qquad 0 \le g \le 1$$

$f$ = plasma frequency,

$f_c$ = critical frequency,

$f_s$ = starting frequency

$T^*_i$ = shifted Chebyshev polynomial [Snyder, 1966]

$A_{I+1}$ = layer half thickness, $Z(f_c) - Z(f_s)$,

$$= - \sum_{i=0}^{I} A_i \; ; \qquad I = 4 \text{ for F region, } I = 2 \text{ for E region.}$$

The coefficients $A_i$ are determined in a least squares fit by minimizing the difference between the $h'_{cal}(f)$ function calculated from equation (1) and the measured $h'(f)$ curve. Huang [1989] has shown that equation (1) is an approximation to a Chapman profile with varying scale height. For the routine calculation of real time profiles a standard POLAN valley is used as proposed by Titheridge [1985], where the valley width W and depth D are a function of the peak height of the E-layer [Reinisch et al., 1989].

Use of a model valley introduces errors in the height of the daytime F layer, especially for plasma frequencies just above foE, the critical frequency of the E layer, when the actual valley shape differs significantly from the model. However, it is often more important to see the diurnal and seasonal variations of the electron density distribution and the effects of solar events and magnetic storms on it than to specify the height with a 10-20 km accuracy. To assess the coupling of the magnetosphere to the F2 ionization and of the mesosphere/thermosphere to the E region, electron contour plots like the one in Figure 9 become invaluable when they are generated for the entire Digisonde network.

Ongoing research tries to resolve the valley ambiguity caused by the fact that no HF waves are reflected from the valley between the E and F regions. Xu et al. [1989] use the change in echo amplitudes for frequencies below and above foE to estimate the valley width W and the depth D. The difference in non-deviate absorption between signals reflected in the F ($f \ge foE$) and the E layer ($f \le foE$) is equal to

$$\Delta L = \frac{e^2}{4\pi^2 mc} \int_{hE}^{hF} \frac{N\nu}{(foE + f_L)^2} \, dh \; [\text{nepers}]$$

where e, m, N are the electron charge, mass and density, ν is the effective collision frequency assumed to vary exponentially with height over the valley region, and $f_L$ is the longitudinal component of the gyrofrequency. By measuring ΔL, an estimate can be made of the electron distribution in the valley region hE < h < hF. We are currently investigating an iterative approach to determine both hF, the height of the first F reflection for f ≥ foE, and the valley ionization $N_V$.

Initial work has started with Digisonde data from Millstone Hill and the calculated profiles are compared with the profiles obtained with the Millstone Hill incoherent scatter radar [Buonsanto, 1989]. The initial differences between the ISR radar and the Digisonde profiles calculated with the standard POLAN valley are illustrated in Figure 11 which shows the lower portion of the noontime electron density profile over Millstone Hill for 10 December 1988. The ISR profile was calibrated with the the foE and hmE values from the Digisonde, so the profiles agree well up to hmE. But the F layer heights of the Digisonde profile are too low by about 15 km since the standard (model) valley is too shallow. Since ARTIST outputs the complete h'(f) traces it is always possible to recalculate the profiles using different inversion algorithms.

## 5. DIGISONDE DRIFT OBSERVATIONS

Spaced-antenna HF observations of ionospheric drifts is an effective method of studying the structure and the dynamics of the ionosphere. In the drift mode the Digisonde operates at 1, 2 or 4 frequencies and records the spectra of the signals received at four or seven receiving antennas. The principal idea [Pfister, 1974] of this drift technique is similar to that of a multibeam radar. The widebeam transmit antenna illuminates an area of several hundred kilometer diameter in the ionosphere. Echoes will be returned to the sounder from all points on the isodensity surface $f_N$ = f, where the surface vector points toward the sounder (neglecting refraction effects). In the presence of any undulations or irregularities more than one reflection point exists; and since there are generally many more than three reflection points, each with a distinct Doppler shift, one can construct the three-dimensional drift velocity vector for the ionospheric motion when the following conditions are satisfied: one, the drift velocity is uniform over the illuminated area, and two, refraction effects can be neglected.

It is important to realize that closely spaced reflection points in the ionosphere cannot be separated with interferometric techniques considering the receiving array dimensions of typically 100 m. For a 10 MHz signal, the 6 dB beam width is about 15°, and correspondingly larger for lower frequencies. To circumvent this difficulty, the Digisonde Fourier analyzes each individual antenna signal [Bibl and Reinisch, 1978], thus separating the different arriving waves in the spectral domain. The discrete Fourier transform determines the complex spectrum ($A_{ij}$, $\phi_{ij}$), with j = 1, . . , 128 (128 spectral lines) and i = 1, . . ., 4 or 7 (for four or seven receiving antennas). The spectral index j gives the Doppler frequency d. The echo arriving from source s has a Doppler shift.

$$d_S = \frac{1}{\pi} \mathbf{v} \cdot \mathbf{k}_s \,, \; s = 1, 2, \ldots \text{ (source number)} \tag{2}$$

where v is the drift velocity and $\mathbf{k}_S$ the wave vector pointing from reflection point s to the receiving antennas. From the spectral phases $\emptyset_{iS}$, the wave vector $\mathbf{k}_S$ is determined, i.e. the source (reflection point) of the wave with Doppler $d_S$. The intersection of the vectors - $\mathbf{k}_S$ with the horizontal plane at the altitude of the radar range (height gate) of the observation generates the so-called skymaps [Bibl et al., 1975].

Figure 12 shows a sequence of four consecutive skymaps, the overhead position is in the center of the map and zenith angles up to 40° are indicated by tick marks at 5° intervals. These measurements were made at Millstone Hill on 11 March 1989 with the sounding frequency f = 3.125 MHz. Each skymap is the result of a 20 second integration, corresponding to a Doppler

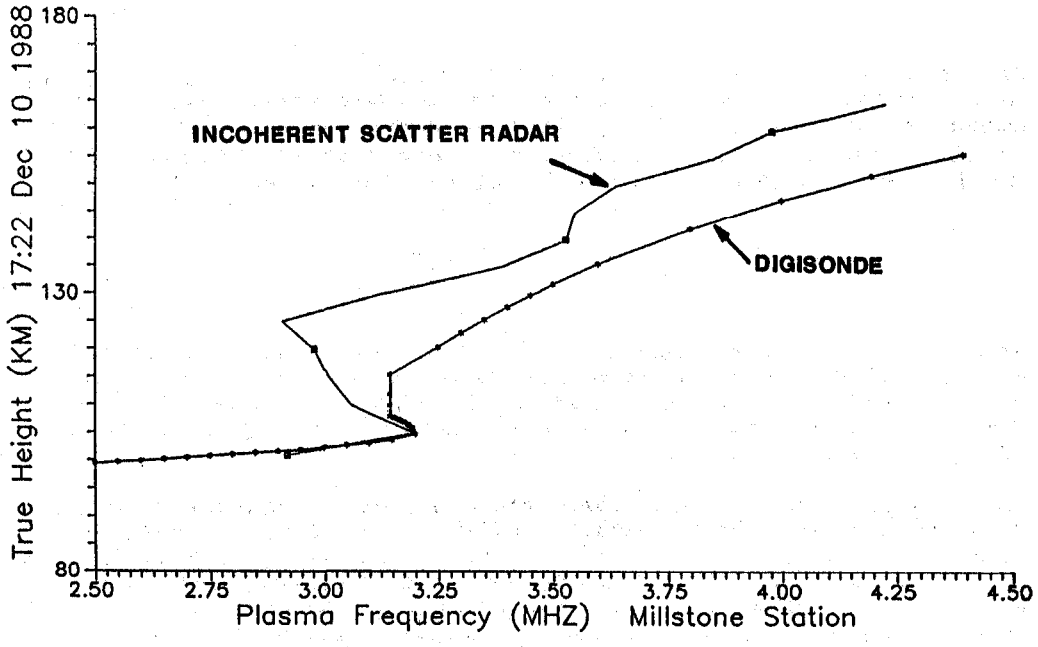


Figure 11 -- Comparison of electron density profiles in the E and lower F regions as measured by Digisonde and incoherent scatter radar. Agreement is quite close up to foE but the E region valley uncertainties cause discrepancies in the F region heights. This data is from Millstone Hill at 12:22 LT on 10 December 1988.

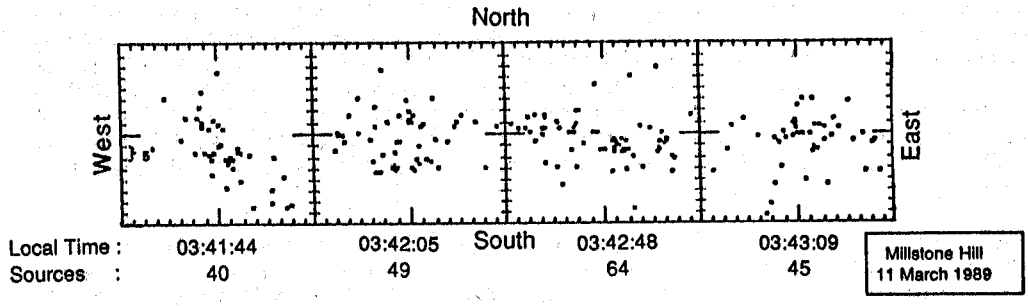


Figure 12 -- Skymap sequence from Millstone Hill depicting sources located during four successive 20 second long measurements. Local time and total number of sources in each skymap are shown. Each point represents a wave component of significant amplitude whose location indicates the arrival angle (azimuth and zenith) of a reflected signal. The center of the skymap is overhead while the middle of each edge corresponds to a 40° zenith angle.

resolution of 0.05 Hz. The sources in these skymaps are widely dispersed, filling most of a ±40° cone above the station. Indicated below each skymap are the local time of the measurement and the number of sources present simultaneously. With the radial velocity $v_{RS} = \pi d_S/k = c d_S/2f$ given at a number of source points the plasma bulk velocity v can be calculated. A least-squares fitting procedure is applied to determine the three components of the velocity vector:

$$\text{Min } \varepsilon^2 = \sum_{s=1}^{S} \left[ d_s - \frac{1}{\pi} \left( v_x k_{sx} + v_y k_{sy} + v_z k_{sz} \right) \right]^2 \qquad (3)$$

where S is the total number of source points which must be 3 or larger to get a solution. The technique breaks down when there are less than three sources, when the velocities become very small, or when the sources are very tightly clustered. For routine drift analysis the individual skymaps are superimposed for 5 minute intervals (see Section 7) assuming that the bulk plasma velocity is constant during this time.

The observed drift for 10-11 March 1989 at Millstone Hill shows a consistent westward drift (Figure 13, lower panel) during nighttime until 0315 LT, when it starts to rotate clockwise (through north) making two full cycles within 4 hours. The horizontal velocity (middle panel) varies between 40 and 220 m/s, reaching its minimum in the early morning hours when the drift vector is rotating. About one hour earlier the vertical velocity $v_Z$ (upper panel) reaches a maximum of 17 m/s downward. The error bars are generally small during nighttime when the ionosphere is rough and many reflection points exist (disturbed ionospheric conditions caused some bad measurements around local midnight). During daytime hours the error bars on the drift direction become large. This is typical for mid-latitude, where the ionospheric roughness (see Section 7) during the day is small, and the few reflection points are clustered in a relatively small area.

The situation is more favorable in the polar cap where the roughness is always sufficiently large to continuously sustain a large number of reflection points, as illustrated in Figures 14 and 15 for data from Qaanaaq, Greenland (87° N corrected geomagnetic) for summer and winter, respectively. The data for 25-27 June 1989, when the ionosphere was continuously sunlit, show very small error bars. The lower panel in Figure 14 shows again the drift direction as a function of time; the azimuth is measured from corrected geomagnetic north. For reference the antisunward direction is indicated, and it is evident that the plasma flow is essentially antisunward, with the exception of a few hours around 09 UT on 25 and 27 June. This is the typical signature of the polar cap two cell plasma convection for IMF $B_Z$ south [Heppner and Maynard, 1987]. The measured horizontal flow velocities vary between 150 and 800 m/s, and the vertical velocities stay generally between ±40 m/s. A more irregular pattern exists during the three winter days in January 1989, displayed in Figure 15. There is clear sunward motion on January 4 from 03 to 23 UT which is generally ascribed to positive $B_Z$ IMF conditions. The highest speeds are observed during periods of antisunward convection.

Several years of Digisonde drift observations at Qaanaaq and at Goose Bay, an auroral station at 65° N CG, have brought convincing evidence that this ground-based technique is monitoring the high latitude convection pattern [Buchau et al., 1988]. This has been further quantified by statistical analyses of the 1986, 87 and 88 Qaanaaq data in relation to the IMF components $B_Z$ and $B_Y$ [Cannon et al., 1989a, 1989b]. These studies show excellent agreement with the two cell model of Heppner and Maynard [1987]. For $B_Z$ south and $B_Y$ negative the average convection direction is rotated anticlockwise from the antisunward direction (Figure 16). For $B_Z$ south and $B_Y$ positive the average convection direction is rotated clockwise (Figure 17). The convection direction when $B_Z$ is north has also been examined. When $B_Z$ is north and $B_Y$ negative the statistical significance of our results is low but the measurements support a severely distorted two cell convection model. For $B_Z$ north and $B_Y$ positive no well defined convection direction can be discerned. The velocity shears in the vicinity of sun aligned polar arcs that are frequently observed during this latter conditions [Carlson et al., 1984] could invalidate our analysis technique. To

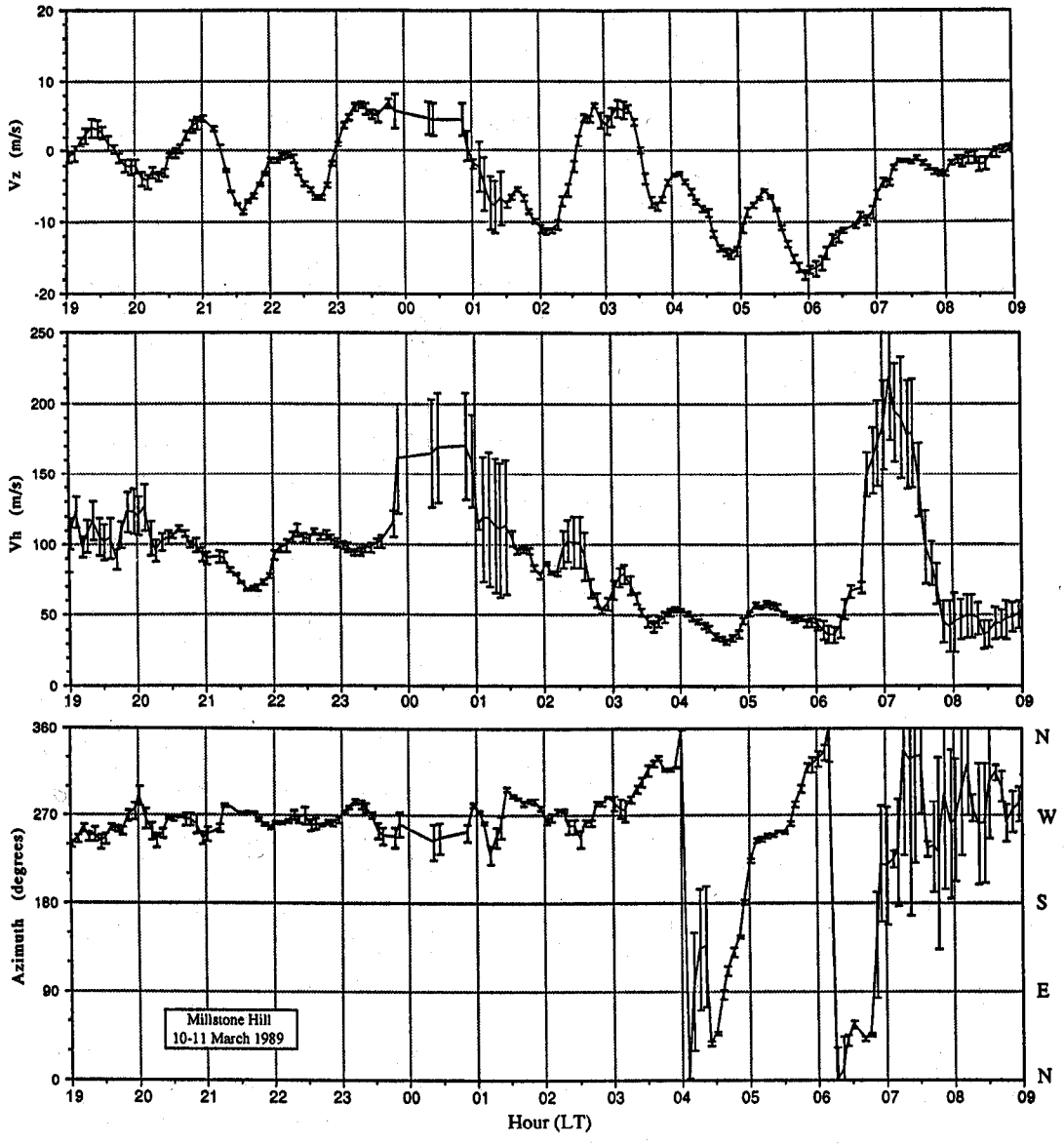


Figure 13 -- Drift velocity vector vertical (top), horizontal magnitude (middle) and azimuthal direction (bottom) components for Millstone Hill on 10-11 Mar 89. Velocity vectors are calculated every 5 minutes using five 20 second long measurements. Sparse data from 23:45 LT to 01:30 LT produce large uncertainties in the velocity. Sunrise occurs at 06:05 LT, after which the drift directions become uncertain.

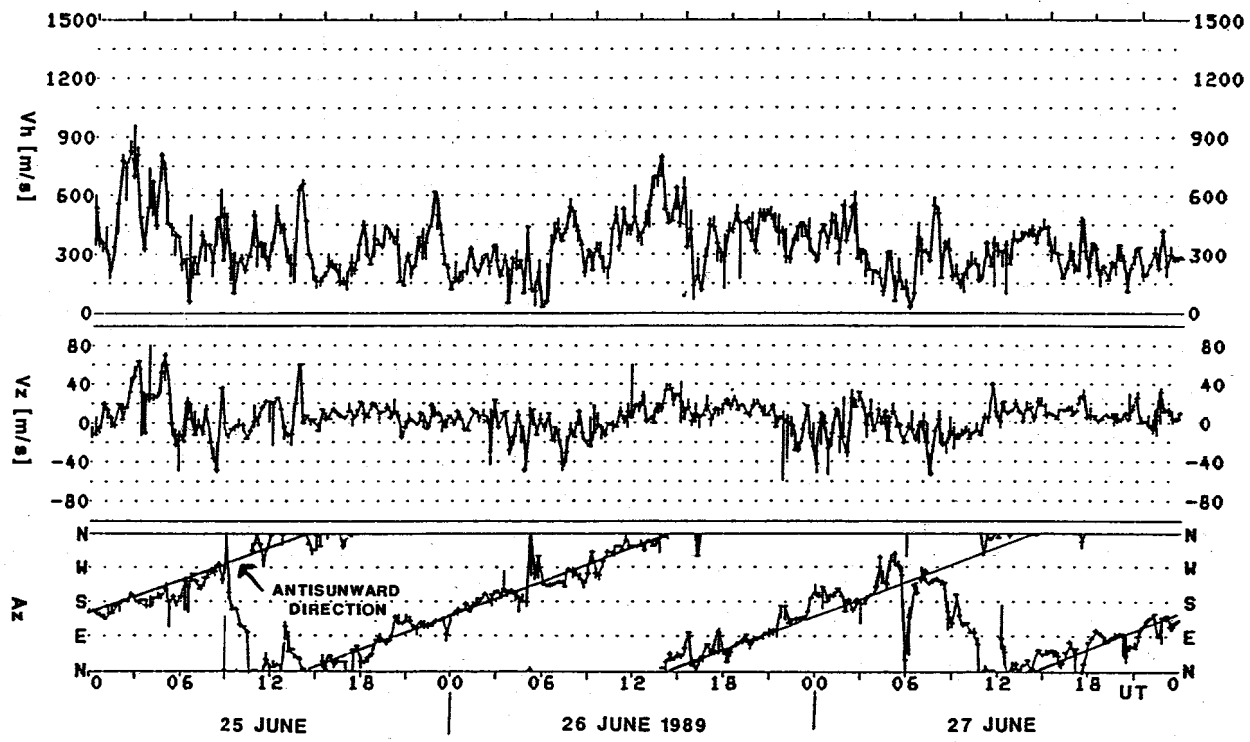


Figure 14 -- Time sequence of drift velocities measured by the Digisonde 256 at Qaanaaq, Greenland on 25-27 June 1989. Top, middle and bottom panels show the horizontal magnitude, the vertical component and the azimuthal direction respectively. Velocities are calculated every 15 minutes. The oblique lines in the bottom panel indicate the approximate antisunward direction. The plasma flow is essentially antisunward most of the time during these three days.

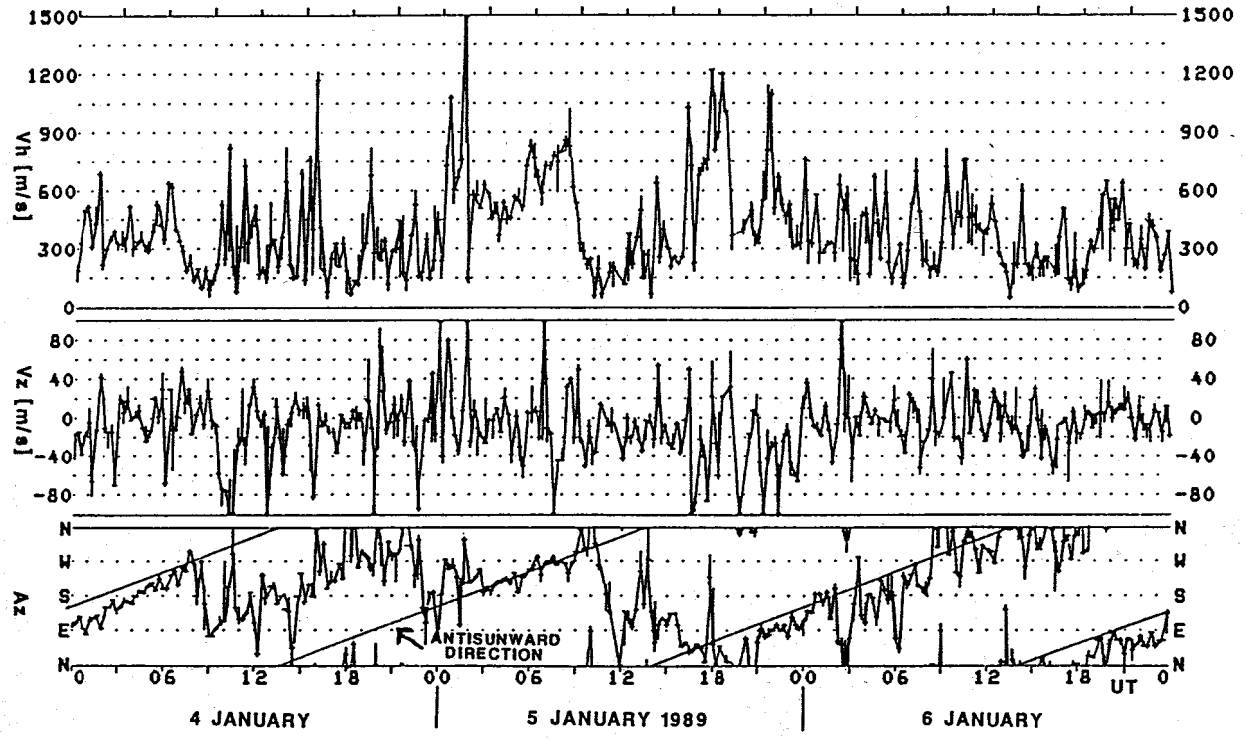


Figure 15 -- Time sequence of drift velocities measured by the Digisonde 256 at Qaanaaq, Greenland on 4-6 January 1989. Top, middle and bottom panels show the horizontal magnitude, the vertical component and the azimuthal direction respectively. Velocities are calculated every 15 minutes. The oblique lines in the bottom panel indicate the approximate antisunward direction. The plasma flow during these three days often diverges from the antisunward direction. Sunward flow predominates between 09 to 23 UT on 4 January.

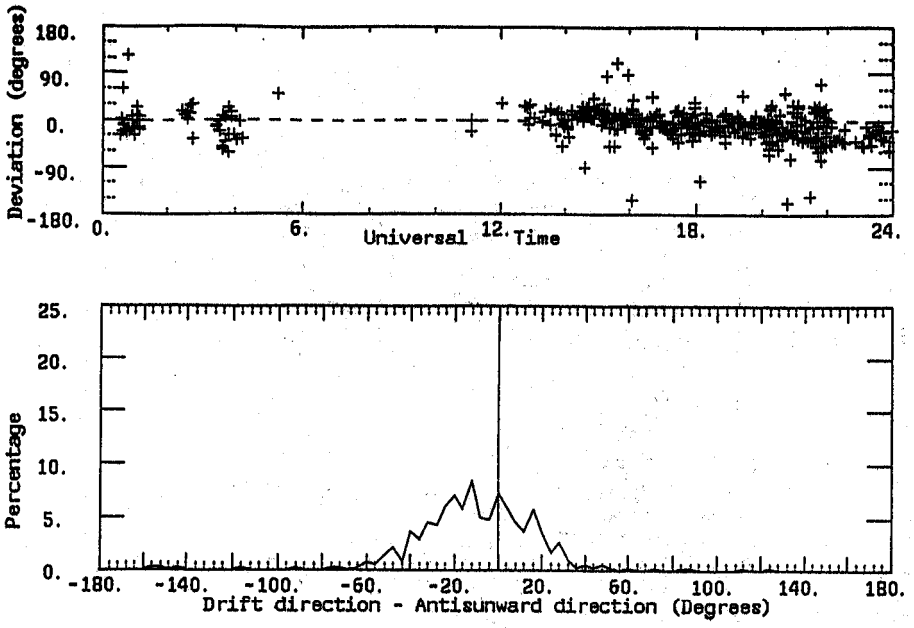


Figure 16 -- Deviation of the drift direction from the anti-sunward when Bz<0 and By < 0: top panel, temporal distribution of selected data, bottom panel, deviation of convection direction from the anti-sunward. The data was selected from 32 days of measurements in 1986,87 and 88 when the interplanetary magnetic field was stable .

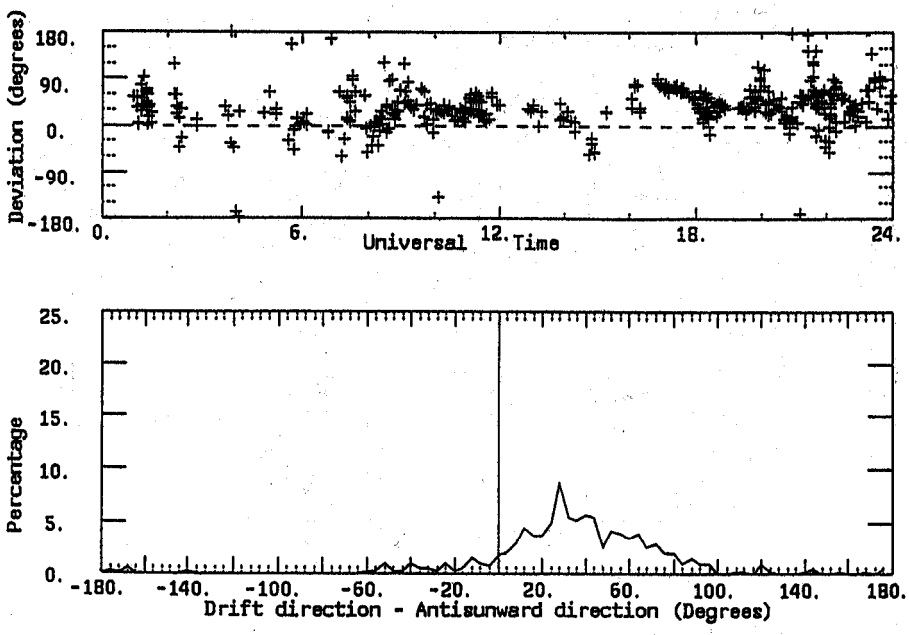


Figure 17 -- Deviation of the drift direction from the anti-sunward when Bz<0 and By > 0: top panel, temporal distribution of selected data, bottom panel, deviation of convection direction from the anti-sunward. The data was selected from 32 days of measurements in 1986,87 and 88 when the interplanetary magnetic field was stable .

properly analyze the Digisonde drift data during $B_Z$, $B_Y$ positive conditions requires all-sky images of the subvisual arcs [Weber et al., 1984] that specify the location of the arcs.

At auroral latitudes, e.g. Goose Bay, the two cell convection pattern is mainly observed during the nighttime, when the clearly defined westward drift changes through south to an eastward drift at about local magnetic midnight. Of course what happens is that Goose Bay is rotating from the dusk cell through the Harang discontinuity to the dawn cell [Buchau et al., 1988]. The flow velocity reaches its minimum (upper panel in Figure 18) in the Harang discontinuity. It is interesting to note that the flow velocity increases rapidly from about 30 m/s to 300 m/s when Goose Bay moves into the trough. In the auroral oval the velocities decline rapidly reaching the values previously observed equatorward of the trough. The arrival times of the trough and the oval at Goose Bay are easily determined on the ionogram surveys discussed in Section 3.

## 6. GRAVITY WAVE STUDIES

Ionogram surveys (Figure 8) and electron density contour plots (Figure 9) are basic tools for the detection and identification of the traveling ionospheric disturbances associated with atmospheric gravity waves (AGW). The contour plots give the wave amplitude and period, but the wavelength and the tilt of the wave front cannot be obtained from the contour plot which presents the electron densities as function of time, not of horizontal distance. To determine the true wavelength, the velocity and the propagation direction of an AGW requires finding the instantaneous electron density surface over a horizontal extend comparable to its wavelength. The incoherent scatter radar could in principle make such measurements,but the acquisition and operating costs render these instruments unsuitable for global gravity wave studies and they also are too slow to do scanning.

The spaced-station technique (Figure 19) deploying several ionosondes separated by 50 km to a few hundred kilometers can determine the AGW parameters. In principle, clusters of analog ionosondes are quite adequate for this task, however, the logistics involved in synchronously running these many sounders and processing all the data are enormous. Also the presence of small and middle scale AGWs can introduce large errors.

Analysis of the Digisonde's drift mode data can lead to the calculation of the true wavelength and velocity of the AGW. We are currently trying to fit a set of sinusoidal surfaces through the observed source points for a given sounding frequency (i.e. plasma frequency) in an effort to determine the wavelengths and the orientations of these wave structures (Figure 20). The velocities can in principle be found from the Doppler frequencies of the source points, however the results may be flawed in the presence of plasma drift. More research is required to resolve this difficulty. Calculating the phases of the AGW, relative to the sounder zenith position, for different plasma densities allows one to determine the tilt of its wave front.

## 7. IONOSPHERIC TILT MEASUREMENTS

Oblique ionospheric HF propagation characteristics are relatively sensitive to horizontal gradients in ionization near the reflection region, since the resulting tilts affect the skip distance and the associated maximum usable frequency (MUF) [Munjal and Sales, 1987]. The Digisonde, operating in the drift mode, can measure the ionospheric tilt. Combining the tilt and vertical profile information improves the predictability of the optimum working frequency for a particular radio path, whether it be for communication or for over-the-horizon radar application. The new tilt technique described here also measures the irregularity structure or "roughness" of the ionosphere. Any theory dealing with the dynamic processes in the upper atmosphere should consider these measured variations in the ionospheric roughness.

Section 5 has discussed the skymaps generated from the Digisonde drift mode data. Each map locates the reflection points (sources) for a coherent dwell, typically 20 sec at mid-latitude. For the tilt and roughness analysis, all 20 sec skymaps for a 5 min observation period are superimposed resulting in a composite skymap. This sampling rate can resolve the effects of acoustic gravity

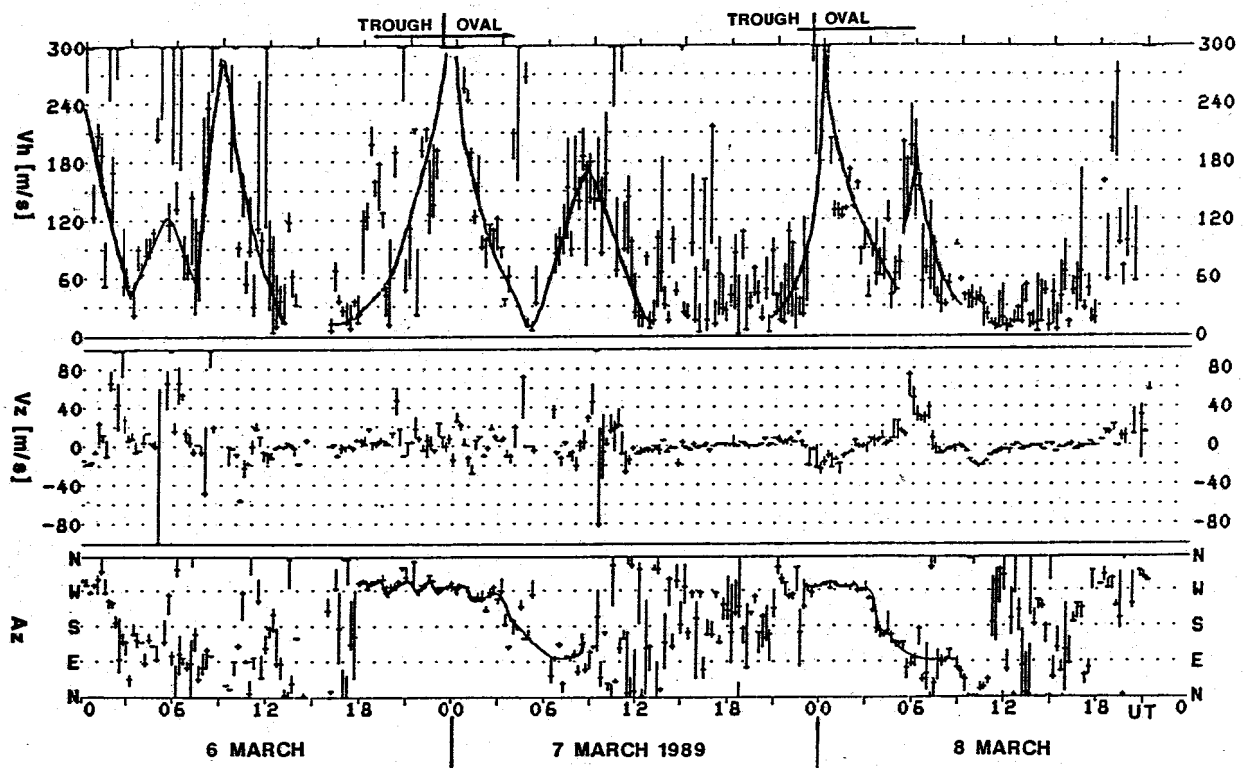


Figure 18 -- Time sequence of drift velocities measured by the Digisonde 256 at Goose Bay, Labrador on 6-8 March 1989. As Goose Bay enters the trough in the evening sector, the drift speed (top panel) increases until the auroral oval is entered. The drift direction (lower panel) is usually stable during the evening hours. The change from westward to eastward drift direction occurs close to local magnetic midnight (0330 UT) and coincides with very small drift magnitudes.

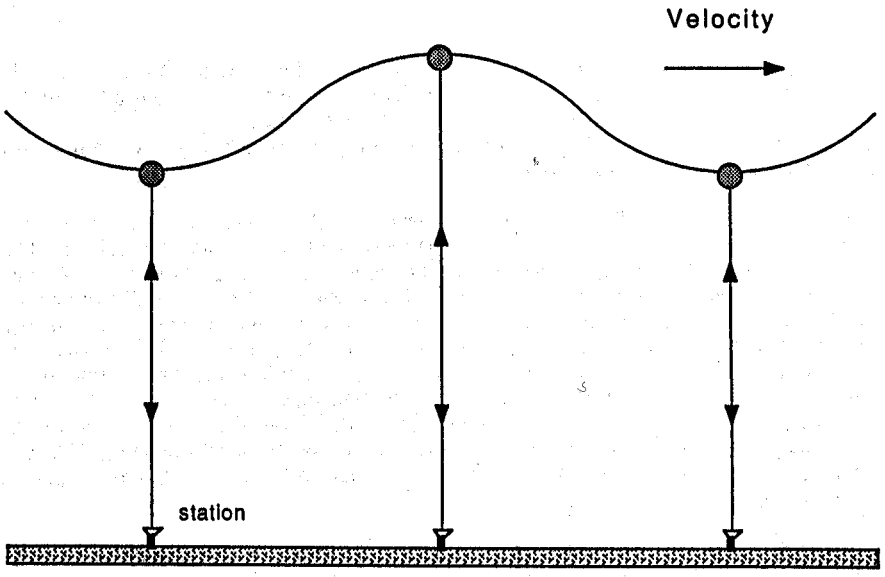


Figure 19 -- Spaced station technique for observing atmospheric gravity waves. Multiple stations simultaneously measure overhead electron density distributions. Comparison of data from coordinated stations can determine the amplitude, phase, wavelength and velocity of the gravity wave.

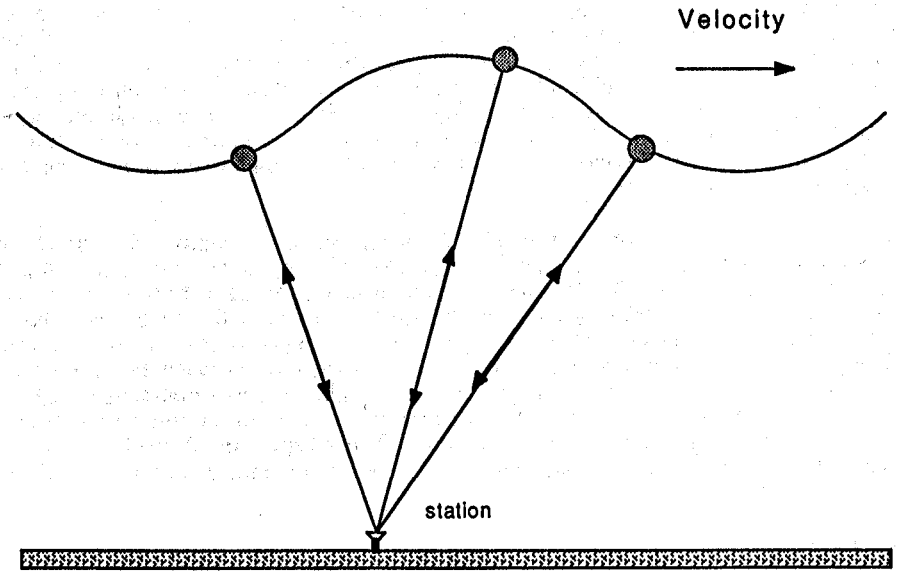


Figure 20 -- Single station technique for observing atmospheric gravity waves. In the drift mode a single Digisonde 256 measures the Doppler shift and arrival angle of signals from multiple reflection points along the wave. This can lead to the calculation of he amplitude, phase, wavelength and velocity of the gravity wave.

waves passing over the site. Figure 21 shows sample composite skymaps for Millstone Hill. The upper half illustrates the concentration of the sources in a very narrow angular region during daytime. During nighttime (lower half of Figure 21) the situation is quite different: the angular locations of the sources are widely spread over the "sky," often out to 30° for mid-latitude, and more in the auroral and polar cap regions.

These representative maps highlight the diurnal variation in the structure, or the roughness, of the reflecting layer. To quantify the spread of the sources we will later define a roughness index. The concept of a tilt of an isodensity surface is well defined during the daytime when all the echoes arrive within a narrow angular cone. The center of this cone, determined as the center of gravity (CG) of the skymap points, specifies the "average" reflection point marked as CG in Figure 21. The CG is displaced from the overhead position in the presence of a tilt. This displacement will occur even when the source distribution is very wide. The angle between the zenith and CG gives the tilt of the layer, and the angle between true north and the vertical plane through the sounder and CG defines the azimuthal orientation (bearing) of the tilt. Figure 22 is a data sample for three consecutive days showing the diurnal variations of the tilt angle and tilt bearing. These data are inherently noisy and the routine presentation of these data uses a one hour (12 point) running average to produce the smooth plots.

We expect to find a diurnal variation of the tilt in addition to any variations caused by AGWs passing over the site. This diurnal variation can be seen for some of the data in the above example. There are clear changes associated with the occurrence of sunset and sunrise in the ionosphere above the Digisonde site. The large cyclical variations in the tilt bearing during the night period were not expected and research is needed to understand the mechanism for these changes. The tilt angles vary from small tilts of of the order of one degree or less to a typical nighttime average of about 4°. These larger nighttime tilts may be related to the dominance of long period AGWs at these times.

Having located the CG of the distribution of reflecting sources we can now measure the spread of the sources about the CG point. We divide the skymap into eight equal angular sectors (45° each) about the CG as the origin. Within each sector a circular arc is drawn about the CG with radius such that one half of the points within the sector lie outside and the other half lie within this arc. These eight arcs define a curve which surrounds one half of all the sources on the particular skymap, and the measure of the solid angle in steradians (SR) of the area inside this curve is defined as the Roughness Index (RI). In order to avoid some peculiarities caused by a small number of points in a particular sector we have introduced a weighting factor proportional to the number of points in the particular sector.

The plot of the smoothed RIs for 3 consecutive days is presented in Figure 23. The RI varies from a value of less than 10 SR in the daytime to a considerably higher values at night, often reaching numbers greater than 100 SR. The daytime clustering of the reflection sources into a small angular area is best described as a smooth ionosphere with a low RI. In contrast, the night ionosphere with high RIs, corresponding to a spread distribution of sources, is characterized as rough. Using models of the irregularity structure makes it possible to determine the scale sizes that are likely to be associated with the changes in the ionosphere from smooth to rough. Our preliminary work indicates, as expected, a good correlation between the nighttime roughness increase and spread-F conditions. Future capabilities of the Digisonde will make it possible to simultaneously measure the tilt and roughness parameters at all heights from the E-region up to near the F-layer peak.

Acknowledgement

This research was in part supported by the Air Force Geophysics Laboratory. The authors thank J. Buchau for his cooperation and numerous informative discussions. The Digisonde data at Goose Bay were collected by Canadian Marconi (B. Gill), and at Qaanaaq by the Danish Meteorological Institute (S. E. Ascanius). We thank R. R. Gamache, C. G. Dozois, P. S. Cannon and G. Crowley for their assistance in preparing this paper.

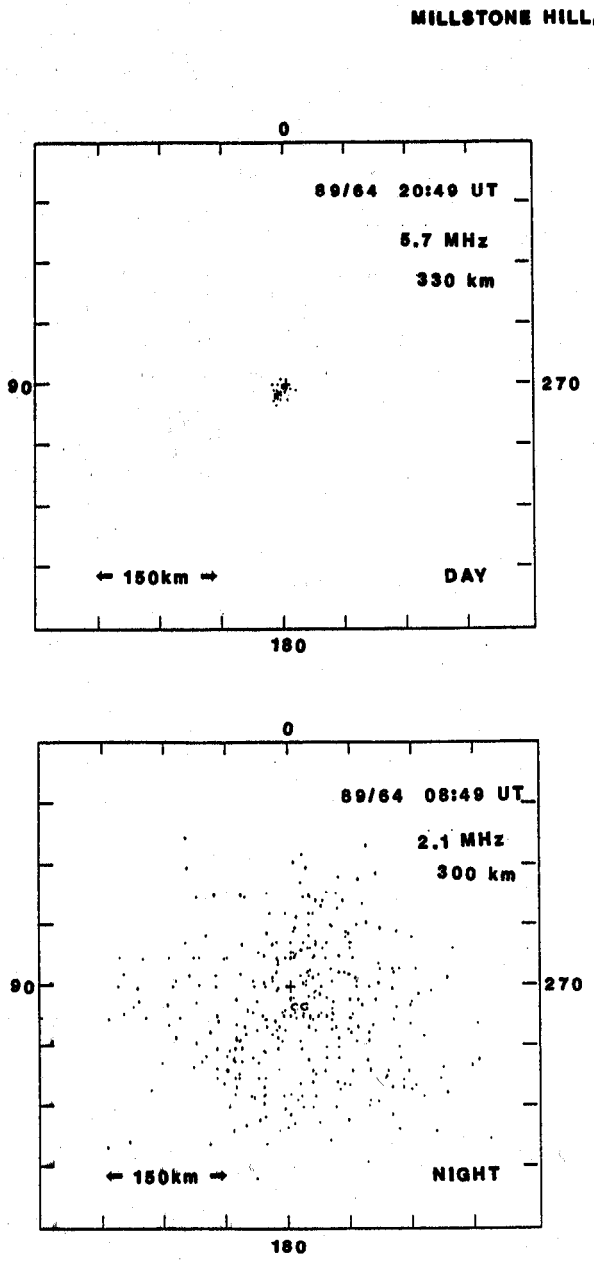


Figure 21 -- Sample skymaps from the ULCAR Digisonde site at Millstone Hill, Westford, MA. The upper panel shows a typical daytime map where all the sources fall within a very small reflecting area. The lower panel is a typical nighttime map showing the increased spread in the angular location of the reflection sources. The center of gravity of all the source points are indicated with the "CG" symbol on each map.

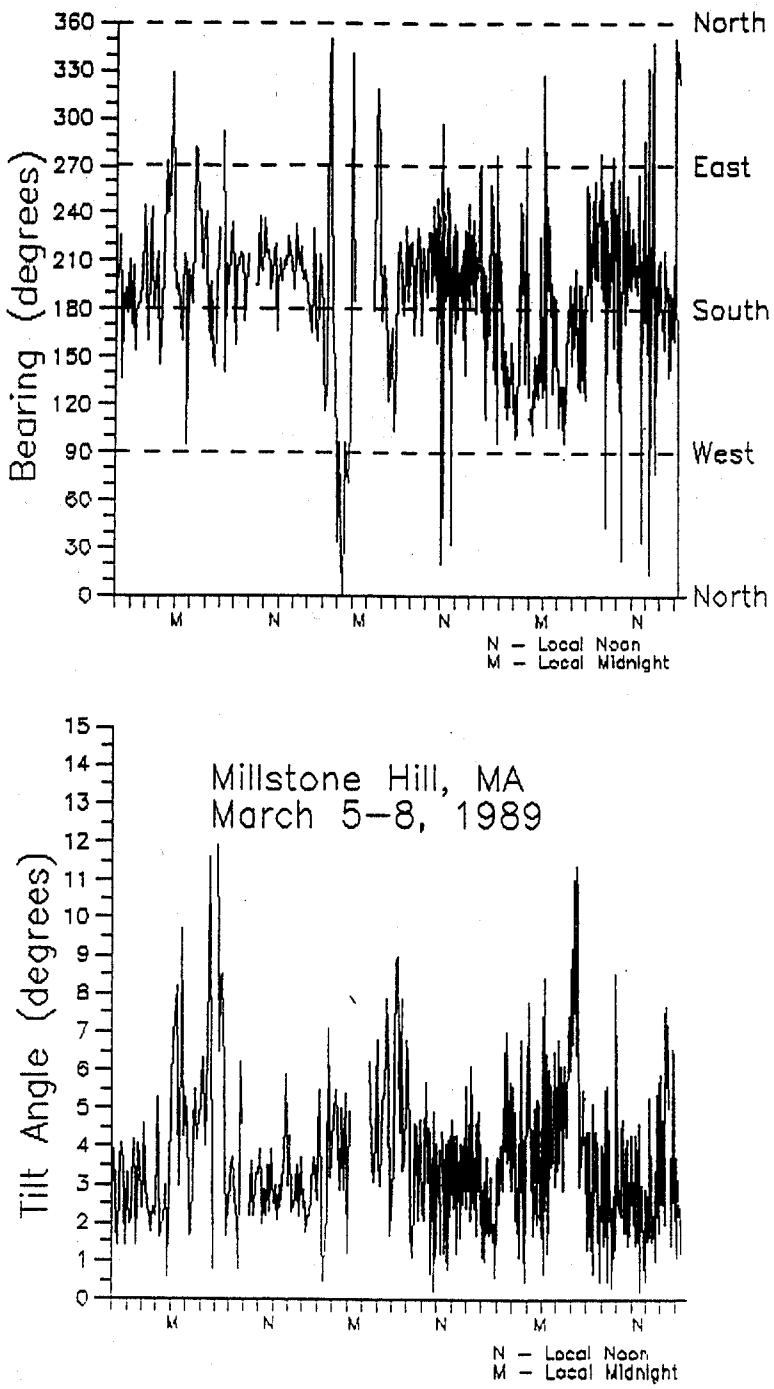


Figure 22 -- Data sample from the ULCAR Digisonde site at Millstone Hill showing the diurnal variation of the tilt angle and bearing for a three day period of data with no smoothing.

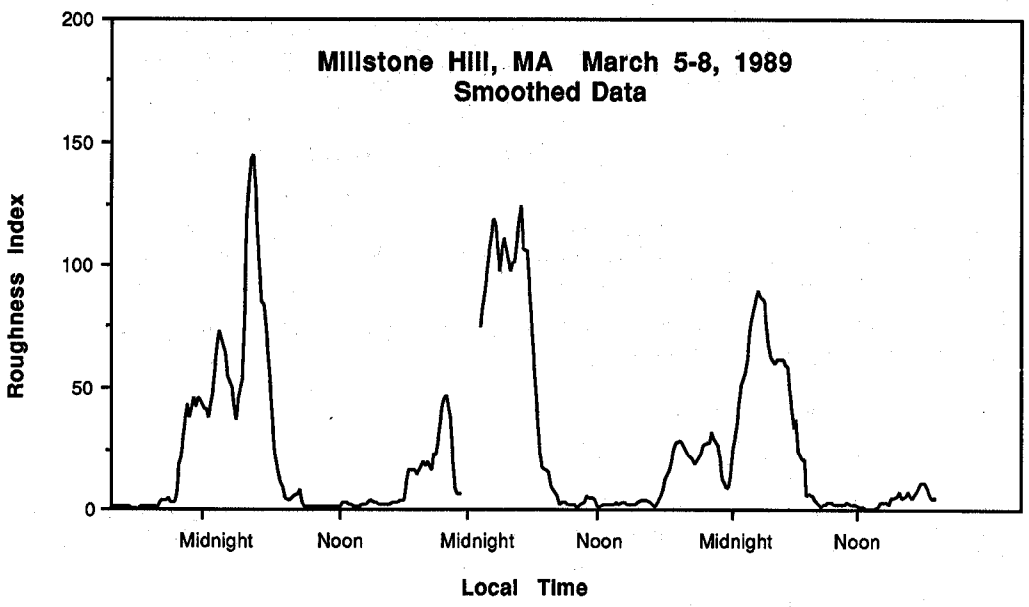


Figure 23 -- The smoothed variations of the roughness index (RI) is shown for the same three days as above. Each day shows a strong diurnal variation of the RI. The roughness index measures the solid angle for the area of the reflecting sources for each five minute period.

REFERENCES

Bibl, K., W. Pfister, B. W. Reinisch and G. S. Sales, 1975, "Velocities of Small and Medium Scale Ionospheric Irregularities Deduced from Doppler and Arrival Angle Measurements," COSPAR, Space Research XV, pp. 405-411.

Bibl, K. and B. W. Reinisch, 1978, "The Universal Digital Ionosonde," Radio Science, 13, No. 3, pp. 519-530

Bibl, K., B. W. Reinisch and D. F. Kitrosser, 1981, "Digisonde 256 - General Description of the Compact Digital Ionospheric Sounder," First Edition, University of Lowell Center for Atmospheric Research.

Breit, G. and M. A. Tuve, 1926, "A test of the existence of the conducting layer," Phys. Rev., 28, 554.

Buchau J., D. N. Anderson, E. J. Weber, B. W. Reinisch and C. G. Dozois, 1988, "Polar Cap Plasma Convection Measurements and Their Relevance to the Real Time Modeling of the High Latitude Ionosphere,".Radio.Science, 23, No. 4, 521.

Buchau, J., B. W. Reinisch, E. J. Weber and J. G. Moore, 1983, "Structure and dynamics of the winter polar cap F region," Radio Science, 18, No. 6, pp. 995-1010.

Buchau, J., 1989, private communication.

Buonsanto, M., 1989, private communication.

Cannon P. S., B. W. Reinisch, J. Buchau, T. Bullett, and C. Dozois, 1989a, "Digital Ionosonde Measurements of High Latitude Ionospheric Convection," Proceedings of IAGA Scientific Assembly, July 1989.

Cannon P. S., B. W. Reinisch, J. Buchau and T. Bullett, 1989b, "A Statistical Validation of the Digisonde Technique for Polar Cap F-Region Convection Measurements.", Submitted to J. Geophys. Res. 1989.

Carlson, H. C., Jr., V. B. Wickwar, E. J. Weber, J. Buchau, J. G. Moore and W. Whiting, 1984, "Plasma characteristics of polar cap F layer arcs," Geophys. Res. Lett., 11, p. 895.

Heppner, J. P. and N. C. Maynard, 1987, "Empirical High-Latitude Electric Field Models, "J Geophys. Res., 92, A5, 4467-4489.

Huang, Xueqin and B. W. Reinisch, 1982, "Automatic Calculation of Electron Density Profiles from Digital Ionograms. 1. Automatic O and X Trace Identification for Topside Ionograms," Radio Science, 17, No. 2, pp. 421-434, March-April 1982.

Huang, Xueqin, 1989, "A Layer Model of the Profile-Fitting Method for Real Time Reduction of Digital Ionograms" (to be published).

Kuklinski, W. S., K. Chandra and B. W. Reinisch, 1988, "Status of DORIS Automatic Scaling, Interim Technical Report, NorthWest Research Associates, Inc., Bellevue, WA.

Munjal, M. and G. S. Sales, 1987, "Improved OTH-B Radar Targeting Using Real-Time Ionospheric Profile Measurements," RADC Technical Report (to be published).

Piggott, W. R. and K. Rawer, 1972, U.R.S.I. Handbook of Ionogram Interpretation and Reduction, Rep. UAG-23, 2nd ed., World Data Center A, Natl. Oceanic and Atmos. Admin., Boulder, CO.

Reinisch, B. W., 1986, "New Techniques in Ground-Based Ionospheric Sounding Studies," Radio Science, 21, No. 3, pp. 331-341.

Reinisch, B. W., K. Bibl, M. Ahmed, H. Soicher, F. Gorman and J. C. Jodogne, 1984, "Multipath and Doppler Observations During Transatlantic Digital HF Propagation Experiments," AGARD Conf. Proceedings, 363, 12-1 to 12-11.

Reinisch, B. W., J. Buchau and E. J. Weber, 1987, "Digital Ionosonde Observations of the Polar Cap F Region Convection," Physica Scripta, 36, pp. 372-377.

Reinisch, B. W., R. R. Gamache and L. G. Bossy, 1989, "Ionospheric Characteristics for IRI in Real Time," Adv. in Space Res., in print.

Reinisch, B. W., R. R. Gamache, X. Huang and L. F. McNamara, 1988, "Real Time Electron Density Profiles from Ionograms," Adv. in Space Res. 8, 4, pp. (4)63-(4)72.

Reinisch, B. W. and Xueqin Huang, 1983, "Automatic Calculation of Electron Density Profiles from Digital Ionograms. 2. True Height Inversion of Topside Ionograms with the Profile-Fitting Method," Radio Science, 18, No. 3, pp. 477-492, May-June 1983.

Snyder, M. A., 1966, Chevyshev Methods in Numerical Approximation, Prentice-Hall, Englewood Cliffs, NJ.

Tang, J., R. R. Gamache and B. W. Reinisch, 1988, "Progress on ARTIST Improvements," Interim Technical Report, NorthWest Research Associates, Inc., Bellevue, WA.

Titheridge, J. E., 1985, "Ionogram Analysis with the Generalized Program POLAN," World Data Center A for Solar Terrestrial Physics, Rep. UAG-93.

Weber, E. J., J. Buchau, J. G. Moore, J. R. Sharber, R. C. Livingston, J. D. Winningham and B. W. Reinisch, 1984, "F-layer ionization patches in the polar cap," J. Geophys. Res. 89, 1683.

Xu, Ling, B. W. Reinisch and M. Buonsanto, 1989, "Ionosonde and Incoherent Scatter Radar Measurements of Vertical Electron Density Profiles," Development of IRI-90 URSI/COSPAR Workshop, Abingdon, England, 7-9 August 1989.